Dark light shining on $B \to K^{(*)} E_{\text{miss}}$

Patrick D. Bolton[*]
Jožef Stefan Institute, Jamova 39, 1000 Ljubljana, Slovenia

Jernej F. Kamenik[†]
Jožef Stefan Institute, Jamova 39, 1000 Ljubljana, Slovenia
and Faculty of Mathematics and Physics, University of Ljubljana, Jadranska 19, 1000 Ljubljana, Slovenia

Martín Novoa-Brunet[‡]
Instituto de Física Corpuscular, Universitat de Valéncia–Consejo Superior de Investigaciones Científicas, Parc Científic, E-46980 Paterna, Valencia, Spain

(Received 9 January 2026; accepted 6 April 2026; published 2 June 2026)

Recent Belle II data on $B^+ \to K^+ E_{\text{miss}}$ show an excess consistent with a two-body decay involving a light invisible particle with mass around 2.1 GeV. We present a UV-complete explanation based on a Higgsed $U(1)'$ gauge symmetry with a light vector boson Z' and a vectorlike top partner, which naturally enhances $b \to s$ transitions. While the minimal model can reproduce the required $B \to K^{(*)} Z'$ rate, it is excluded by LHCb searches for resonant dimuon decays due to unavoidable loop-induced couplings of Z' to charged leptons. We show that a minimal extension with an additional light $U(1)'$-charged singlet fermion allows Z' to decay dominantly invisibly, evades existing constraints coming also from dark photon and collider searches as well as Higgs measurements, and can simultaneously account for the Belle II excess and the observed dark matter abundance through resonant thermal freeze-out.

DOI: 10.1103/68gt-2nlf

I. INTRODUCTION

Rare flavor-changing neutral current (FCNC) transitions in the quark sector provide a powerful window into physics beyond the Standard Model (SM). The loop- and Cabibbo-Kobayashi-Maskawa-suppressed rates predicted in the SM allow us in many cases to probe new short distance dynamics much above the TeV scale. However, new degrees of freedom affecting rare FCNC processes can also appear at or even below the SM weak and QCD scales. The decays $B \to K^{(*)} E_{\text{miss}}$, $D^0 \to \pi^0 E_{\text{miss}}$, and $K \to \pi E_{\text{miss}}$, where the missing energy represents final state particles that escape detection, have recently emerged as sensitive probes of such new physics. In particular, the Belle II Collaboration has reported a 2.9σ excess in $B^+ \to K^+ E_{\text{miss}}$ over SM expectations based on the $b \to s\nu\bar{\nu}$ transition [1]. Even more interestingly, the excess is somewhat concentrated around the (two-body decay) kinematic region corresponding to the missing energy carried away by a single particle with mass of about 2.1 GeV [2].[1]

In Refs. [2,4], we analyzed this excess using a model-independent approach based on the effective field theory (EFT) framework for new light SM singlet fields coupled to quark flavor-changing currents [5] (see also Refs. [6–11] for related work). Among several considered scenarios which can consistently account for the Belle II result, the data give slight preference to the emission of a single spin-0 or spin-1 state, provided its mass and couplings to the quark sector fall within a narrow range. However, the EFT description alone leaves open the question of UV consistency and the microscopic origin of such scenarios. In this work, we try to address this by constructing an explicit, renormalizable new physics model, which matches onto the low energy EFT of a new massive vector field predominantly coupling to $b \to s$ currents. Our model is built on the aligned gauged and Higgsed $U(1)'$ framework with a vectorlike top partner, following the general ideas introduced in Ref. [12]. It is an explicit realization of a rank-1

[*]Contact author: patrick.bolton@ijs.si
[†]Contact author: jernej.kamenik@cern.ch
[‡]Contact author: martin.novoa@ific.uv.es

[1]Very recently, Belle has presented preliminary results of their search targeting resonant $B^+ \to K^+(X \to \text{invisible})$ decays, putting stringent bounds on the two-body decay topology of $B^+ \to K^+ E_{\text{miss}}$ [3]. However, the region of resonant masses $m_X \sim 2$ GeV preferred by our analysis [2] is vetoed due to overwhelming SM backgrounds and thus remains unconstrained.

flavor symmetry breaking [10,13] and naturally implements the minimally flavor-violating approximate $U(2)$ flavor symmetry structure of beyond the Standard Model effects [14–16], predicting the largest contributions to $b \to s$ FCNCs.

Several alternative explanations of the Belle II excess within explicit models have appeared in the literature, targeting both two-body [17–26] and three-body [21,27–43] $B \to K E_{\rm miss}$ decay kinematics. In particular, Ref. [40] considered an SM extension with an unbroken gauged $U(1)'$ symmetry and new light Dirac fermions charged under it. The Belle II excess is then accommodated via off-shell exchange of the massless dark photon associated with this new gauge symmetry, where the dark photon interactions to SM quarks are parametrized by nonrenormalizable effective operators. Reference [21] (see also Ref. [25]) instead considers a similar model, where the extra symmetry is a (Higgsed) $U(1)_{\tau-\mu}$. In this case, the Belle II signal is accommodated via light $U(1)_{\tau-\mu}$ Higgs boson emission (either on or off shell) and subsequent decay to new fermions, also charged under $U(1)_{\tau-\mu}$. The corresponding massive vector boson in this model does not play a relevant role in flavor phenomenology, but is crucial in accounting for correct cosmological dark matter (DM) abundance of the new fermions. Similarly, Ref. [18] briefly considers a Higgsed $U(1)_{B_3-L_3}$, where the emission of the associated light Z' decaying to $\nu_\tau \bar{\nu}_\tau$ pairs accounts for the Belle II excess. Conversely, Ref. [24] considered gauging and Higgsing the anomalous $U(1)_\tau$, where the Z' couplings to SM quarks arise at one loop through the associated Wess-Zumino terms [24]. Finally, Ref. [22] recently considered a Higgsed $U(1)'$ mediating DM interactions, where the associated light Z' appearing in $B \to K^{(*)} E_{\rm miss}$ only interacts with the SM fermions though kinetic mixing with hypercharge.

The main goals of this paper are threefold: first, we present the minimal aligned $U(1)'$ model realization and demonstrate how it could account for the Belle II excess in $B \to K^{(*)} E_{\rm miss}$ through the production of a light massive and invisibly decaying Z'. We also comment on similarities and main differences with existing related proposals [18,22,24]. Second, we analyze the full set of phenomenological constraints on the model, including other flavor observables, electroweak precision data, and collider bounds. Importantly, we show that after electroweak symmetry breaking, irreducible $Z - Z'$ mass mixing induces Z' couplings to all SM fermions and the model is excluded by the LHCb searches for prompt and displaced $\mu^+\mu^-$ resonances in $B \to K^{(*)}\mu^+\mu^-$ decays [44,45]. Third, we investigate a possible minimal extension of the model that avoids the LHCb constraint by introducing an additional light SM singlet fermion charged under the $U(1)'$, and thus opening new dominant invisible decay channels of the Z'. This additional particle turns out to be a viable DM candidate, and we explore the related phenomenology in detail.

Altogether, our results highlight the potential of UV-complete dark sector models to address the Belle II anomaly while remaining predictive and testable across multiple experimental frontiers.

The remainder of this work is organized as follows: in Sec. II, we introduce the minimal aligned $U(1)'$ model, detailing its field content, gauge and scalar interaction sectors, and the resulting mass and mixing structures. We then study its implications for $B \to K^{(*)} E_{\rm miss}$ at Belle II, together with other closely related experimental constraints. In Sec. III, we study a minimal extension of the model with an additional light SM singlet fermionic field introducing interesting correlations between flavor probes, dark photon and collider searches, electroweak precision observables, and DM phenomenology. We summarize our findings and discuss possible other, nonminimal extensions of the model in Sec. IV.

II. MINIMAL MODEL

Here, we consider a minimal aligned $U(1)'$ model which introduces a vectorlike quark $T'(\mathbf{3},\mathbf{1},2/3,q')$ and an SM singlet scalar $\Phi(\mathbf{1},\mathbf{1},0,q')$, where q' is the charge of both fields under an additional $U(1)'$. The Lagrangian of the model contains

$$\begin{aligned}\mathcal{L} \supset & -\frac{1}{4}B'_{\mu\nu}B'^{\mu\nu} - \frac{\epsilon_B}{2}B_{\mu\nu}B'^{\mu\nu} + |D_\mu \Phi|^2 - V(H,\Phi) \\ & + \bar{T}'(i\not{D} - M_T)T' - \left[y_T^r \overline{T'}\Phi u'_{Rr} + \text{H.c.}\right], \end{aligned} \tag{1}$$

with $D_\mu \supset i\tilde{g}q' B'_\mu$ and $B'_{\mu\nu} = \partial_\mu B'_\nu - \partial_\nu B'_\mu$, where B'_μ is the gauge field associated with the $U(1)'$, B_μ is the $U(1)_Y$ hypercharge gauge field, H the $SU(2)_L$ Higgs doublet, and u'_{Rr} the up-type right-handed quark with generation index $r = u, c, t$. Additional terms in the scalar potential are

$$V(H,\Phi) = -\tilde{\mu}^2|\Phi|^2 + \tilde{\lambda}|\Phi|^4 + \lambda'|\Phi|^2(H^\dagger H). \tag{2}$$

The complex scalar Φ obtains a vacuum expectation value (VEV) $\tilde{v}$ that breaks the $U(1)'$. In the broken phase, the model admits an additional massive vector boson, Z', with the mass $M_{Z'} = \tilde{g}q'\tilde{v}$.

A. Spectrum and theoretical constraints

1. Fermions

In the following, we consider $y_T^t \neq 0$ and $y_T^u = y_T^c = 0$, so that the vectorlike quark T' only mixes with the top quark (and is thus a heavy top partner). In the broken phase, the relevant mass matrix in the top-type quark sector is thus

$$\mathcal{L} \supset -\frac{1}{\sqrt{2}}\begin{pmatrix}\bar{t}'_L & \bar{T}'_L\end{pmatrix}\begin{pmatrix} v y_t & 0 \\ \tilde{v} y_T^t & \sqrt{2}M_T\end{pmatrix}\begin{pmatrix} t'_R \\ T'_R\end{pmatrix} + \text{H.c.}, \tag{3}$$

with y_t the top Yukawa coupling, $\mathcal{L} \supset -y_t \bar{Q}_3 \tilde{H} t'_R + \text{H.c.}$, and where, without loss of generality, y_t, y_T^t, and M_T can be made real and positive by a rephasing of the chiral fields. The resulting mass basis fields can be obtained via the biunitary rotation $t'_X = P_X(c_X t + s_X T)$ and $T'_X = P_X(-s_X t + c_X T)$ for $X = L,\ R$, with $s_X = \sin\theta_X$ and $c_X = \cos\theta_X$, where the left- and right-handed mixing angles are given by

$$\tan 2\theta_{L,R} = \frac{\tilde{v} y_T^t \{v y_t, \sqrt{2} M_T\}}{M_T^2 \pm (\tilde{v} y_T^t)^2/2 - (v y_t)^2/2}, \tag{4}$$

and the physical masses satisfy $m_t m_T = v y_t M_T/\sqrt{2}$ and $m_t^2 + m_T^2 = (v y_t)^2/2 + (\tilde{v} y_T^t)^2/2 + M_T^2$. In the following, $\{m_T, \tilde{g}q', y_T^t\}$ are taken as input parameters, assuming $m_T > m_t$. Using the relation $M_{Z'} = \tilde{g}q'\tilde{v}$, the VEV $\tilde{v}$ can be eliminated in favor of $\tilde{g}q'$ and $M_{Z'} = 2.1$ GeV, with the latter being kept fixed to best fit of the Belle II excess. The top quark Yukawa coupling is given in terms of the input parameters as $v y_t/\sqrt{2} = m_t c_L c_R + m_T s_L s_R$. From the identity $m_t c_L s_R = m_T c_R s_L$, we expect $s_L \ll s_R$ in the limit $m_t \ll m_T$. For $y_T^t \to 0$, $s_{L,R} \to 0$ and t (with $m_t = v y_t/\sqrt{2}$) and T ($m_T = M_T$) decouple.

In most of the viable parameter space, the $t - T$ mixing is given by $s_R \approx s_L m_T/m_t \approx \tilde{v} y_T^t/\sqrt{2} m_T$. However, we can determine the maximal values of $s_{L,R}$ by combining the relations below Eq. (4) with $(M_T - v y_t/\sqrt{2})^2 \geq 0$, yielding $\tilde{v} y_T^t/\sqrt{2} \leq m_T - m_t$, or equivalently

$$\tilde{g}q' \geq \frac{M_{Z'} y_T^t}{\sqrt{2}(m_T - m_t)}. \tag{5}$$

We refer to this as a *consistency* bound, as its violation would imply deviations from the assumed $t - T$ mixing from Eq. (3). The lower bound in Eq. (5) corresponds to the upper limits $s_{L,R}^2 \leq m_{t,T}/(m_t + m_T)$. To remain compatible with perturbative unitarity, the two Yukawa couplings must satisfy $y_t, y_T^t < \sqrt{8\pi/3}$ [46].

Considering next the quark gauge interactions in the broken phase, i.e., $\mathcal{L} \supset -\mathcal{J}_\mu \mathcal{A}^\mu - \frac{g}{\sqrt{2}}[J_\mu^+ W^{+\mu} + \text{H.c.}]$, where $\mathcal{J}_\mu = (e J_\mu, \frac{g}{c_w} J_\mu^Z, \tilde{g} J'_\mu)$ and $\mathcal{A}_\mu = (A_\mu, Z_\mu, Z'_\mu)^T$, the up-type quarks can be rotated to the mass basis. The currents then contain the terms

$$\begin{aligned}
J_\mu &\supset Q_u(\bar{t}\gamma_\mu t + \bar{T}\gamma_\mu T),\\
J_\mu^Z &\supset \frac{1}{2}(c_L \bar{t} + s_L \bar{T})\gamma_\mu P_L (c_L t + s_L T) - s_w^2 J_\mu,\\
J'_\mu &\supset q'(-s_X \bar{t} + c_X \bar{T})\gamma_\mu P_X(-s_X t + c_X T),\\
J_\mu^+ &\supset V_{ti}(c_L \bar{t} + s_L \bar{T})\gamma_\mu P_L d_i,
\end{aligned} \tag{6}$$

where $Q_u = 2/3$, θ_w is the weak mixing angle, and V_{ij} are elements of the Cabibbo-Kobayashi-Maskawa matrix.

2. Gauge bosons

In general, A_μ, Z_μ, and Z'_μ above are not gauge sector mass eigenstates of the model. At tree level, the SM gauge bosons B/W^3 do not mix with B'. The former are rotated to the mass basis fields γ/Z, while B' produces the extra massive field Z'. However, at one loop, kinetic and mass mixing of Z' and γ/Z arises. The kinetic mixing of B' and B is controlled by ϵ_B in Eq. (1), which runs above the vectorlike quark mass M_T according to the renormalization group evolution (RGE) $d\epsilon_B/d\ln\mu = -e\tilde{g}q'/3\pi^2 c_w$. In the unbroken phase, this running is generated by the one-loop exchange of T', which is charged under both $U(1)'$ and $U(1)_Y$. The RGE also applies in the broken phase of the theory, with the mass eigenstates t/T in the loop, as depicted in Fig. 1. We note that in the broken phase, the kinetic mixing ϵ_W is also effectively induced between B' and W^3 from the mixing of upper component of the $SU(2)_L$ doublet Q_3 and T'_L. This is is equivalent to the contribution of the $d = 8$ operator $|\Phi|^2(H^\dagger \tau^3 H) W^3_{\mu\nu} B'^{\mu\nu}$ [47]. The kinetic mixing ϵ_B also receives threshold contributions encoded by $|\Phi|^2 B_{\mu\nu} B'^{\mu\nu}$ at $d = 6$ and $|\Phi|^2(H^\dagger H) B_{\mu\nu} B'^{\mu\nu}$ and $|\Phi|^4 B_{\mu\nu} B'^{\mu\nu}$ at $d = 8$.

For $\epsilon_{B,W} \neq 0$, the kinetic mixing terms in the gauge boson mass basis are $\mathcal{L} \supset -\frac{\epsilon_A}{2} F_{\mu\nu} Z'^{\mu\nu} - \frac{\epsilon_Z}{2} Z_{\mu\nu} Z'^{\mu\nu}$, where $\epsilon_A = c_w \epsilon_B + s_w \epsilon_W$ and $\epsilon_Z = -s_w \epsilon_B + c_w \epsilon_W$ are the θ_w rotated kinetic mixing coefficients. For $\epsilon_B(\mu) \neq 0$ at the high scale $\mu = \Lambda \gg m_T$, $\epsilon_{A,Z}$ are given by

$$\epsilon_A = c_w \epsilon_B(\Lambda) + \frac{e\tilde{g}q'}{6\pi^2}\left[\ln\frac{\Lambda^2}{m_T^2} + \frac{1}{2}(s_L^2 + s_R^2)\ln r\right], \tag{7}$$

$$\epsilon_Z = -t_w \epsilon_A - \frac{g\tilde{g}q'}{16\pi^2 c_w} c_L^2 s_L^2 f(r), \tag{8}$$

where $t_w = \tan\theta_w$, $r = m_T^2/m_t^2$, and

$$f(x) = \frac{5x^2 - 22x + 5}{3(x-1)^2} - \frac{x^3 - 3x^2 - 3x + 1}{(x-1)^3}\ln x. \tag{9}$$

The second term in ϵ_Z arises from threshold effects. In the following, we will mostly assume that $\epsilon_B(\Lambda) = 0$ at the high scale $\Lambda = 10^{16}$ GeV and use the induced values of $\epsilon_{A,Z}$ from the RGE plus threshold corrections. In much of the relevant parameter space, $s_L \ll s_R < 1$, giving $\epsilon_A \approx -\epsilon_Z/t_w \approx 3 \times 10^{-4}(\tilde{g}q'/10^{-3})(L_T/55)$ with

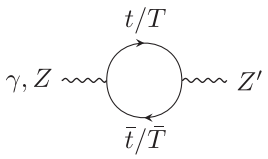

FIG. 1. One-loop contributions of t/T to the kinetic and mass mixing between Z' and γ/Z.

$L_T \equiv \ln \Lambda^2/m_T^2$. We note that ϵ_A may be suppressed if there is a cancellation between $\epsilon_B(\Lambda)$ and the value generated by the running. Even in the presence of this fine-tuning, ϵ_Z would still be generated by the second term in Eq. (8) Finally, in the $y_T^t \to 0$ limit, $\epsilon_A = -\epsilon_Z/t_w = e\tilde{g}q' L_T/6\pi^2$ holds exactly.

After electroweak symmetry breaking, the diagram in Fig. 1 also induces mass mixing between Z and Z'. The effective mass term can be written as $\mathcal{L} \supset M_{ZZ'}^2 Z_\mu Z'^\mu$, from which it is convenient to define the dimensionless quantity $\delta_Z = M_{ZZ'}^2/M_Z^2$. For $m_t \ll m_T$, the one-loop contribution yields

$$\delta_Z = -\frac{3g\tilde{g}q'}{32\pi^2 c_w}\frac{m_t^2}{M_Z^2} s_L^2 \left[c_L^2 g(r) - 2c_R^2 h(r)\right], \quad (10)$$

where $g(x) = 1 + x - \frac{2x}{x-1}\ln x$ and $h(x) = 2x - \frac{x(x+1)}{x-1}\ln x$. The mass mixing can also be viewed as the contribution of the $d = 6$ operator $(H^\dagger D_\mu H)(\Phi^\dagger D^\mu \Phi) + \text{H.c.}$, and is an irreducible effect (cannot be cancelled against a UV parameter) in the model for $y_T^t \neq 0$. Thus, $\delta_Z \to 0$ is only possible for $y_T^t \to 0$, while on the other hand, we need $y_T^t \neq 0$ in order to accommodate the Belle II result via $B^+ \to K^+ Z'$ decays, as we demonstrate in Sec. II B.

The impact of the kinetic and mass mixing can be seen in the low energy interactions of γ, Z, and Z'. With $\epsilon_{A,Z} \neq 0$, the massive gauge fields are not canonically normalized; a nonunitary rotation can first diagonalize the matrix containing the kinetic mixing terms, followed by a unitary rotation diagonalizing the gauge boson mass matrix containing the mass mixing term δ_Z. We obtain the following redefinition of fields: $A_\mu \to A_\mu - \epsilon_A Z'_\mu$, $Z_\mu \to Z_\mu - (\delta_Z - x\epsilon_Z)Z'_\mu$, and $Z'_\mu \to Z'_\mu + (\delta_Z - \epsilon_Z)Z_\mu$, where we expand to leading order[2] in $\epsilon_{A,Z}$, δ_Z and the ratio $x \equiv M_{Z'}^2/M_Z^2 = 5.3 \times 10^{-4}$. Explicitly, the coupling of Z' to fermions is $\mathcal{L} \supset -\bar{f}\gamma_\mu(v_{Z'}^f - a_{Z'}^f\gamma_5) f Z'^\mu$, with the vector and axial-vector couplings

$$\begin{aligned} v_{Z'}^f &= \tilde{g}\mathfrak{v}^f - eQ_f\epsilon_A - \frac{g}{2c_w}\left(T_3^f \vartheta^f - 2s_w^2 Q_f\right)\Delta_{Z'}, \\ a_{Z'}^f &= \tilde{g}\mathfrak{a}^f - \frac{g}{2c_w} T_3^f \vartheta^f \Delta_{Z'}, \end{aligned} \quad (11)$$

where T_3^f is the third component of $SU(2)_L$ isospin, Q_f is the $U(1)_{\text{em}}$ charge, and we define $\Delta_{Z'} = \delta_Z - x\epsilon_Z$. The couplings in Eq. (11) are diagonal in flavor space for $f = \nu, \ell, d, u$ $(i, j \neq t, T)$, with $\mathfrak{v}_{ij}^f, \mathfrak{a}_{ij}^f = 0$ and $\vartheta_{ij}^f = \delta_{ij}$. For up-type quarks with $i, j = t, T$, the couplings can be read off from Eq. (6), i.e.,

$$\begin{aligned} \{\mathfrak{v}_{tt}^u, \mathfrak{a}_{tt}^u\} &= q'(s_L^2 \pm s_R^2)/2, \\ \left\{\mathfrak{v}_{TT}^u, \mathfrak{a}_{TT}^u\right\} &= q'(c_L^2 \pm c_R^2)/2, \\ \left\{\mathfrak{v}_{tT}^u, \mathfrak{a}_{tT}^u\right\} &= \left\{\mathfrak{v}_{Tt}^u, \mathfrak{a}_{Tt}^u\right\} = -q'(s_L c_L \pm s_R c_R)/2, \end{aligned} \quad (12)$$

and $\vartheta_{tt}^u = c_L^2$, $\vartheta_{TT}^u = s_L^2$, and $\vartheta_{tT}^u = \vartheta_{Tt}^u = c_L s_L$. For $\epsilon_{A,Z} \gg \delta_Z$ and $x \ll 1$, the couplings of SM fermions to Z' are effectively proportional to eQ_f, corresponding to the dark photon limit. Instead, for $\epsilon_{A,Z} \ll \delta_Z$, Z' possesses SM Z-like couplings. Consequently, the kinetic and mass mixing determine the Z' lifetime, as examined in Sec. II B. Finally, the modified Z couplings to fermions read $\mathcal{L} \supset -\bar{f}\gamma_\mu(v_Z^f - a_Z^f\gamma_5) f Z^\mu$, with the vector and axial-vector couplings

$$\begin{aligned} v_Z^f &= \frac{g}{2c_w}\left(T_3^f \vartheta^f - 2s_w^2 Q_f\right) + \tilde{g}\mathfrak{v}^f \Delta_Z, \\ a_Z^f &= \frac{g}{2c_w} T_3^f \vartheta^f + \tilde{g}\mathfrak{a}^f \Delta_Z, \end{aligned} \quad (13)$$

where the $\mathfrak{v}^f$, $\mathfrak{a}^f$ and ϑ^f factors are the same as above, and we define $\Delta_Z = \delta_Z - \epsilon_Z$.

3. Scalars

Next, we consider the scalar boson sector of the minimal model. The full scalar potential is minimized for $\mu^2 = \lambda v^2 + \lambda' \tilde{v}^2/2$ and $\tilde{\mu}^2 = \tilde{\lambda}\tilde{v}^2 + \lambda' v^2/2$, where μ^2 and λ are the usual Higgs mass parameter and quartic coupling, $V \supset -\mu^2 H^\dagger H + \lambda(H^\dagger H)^2$, and v is the Higgs VEV. For the scalar potential to be bounded from below, the quartic couplings must satisfy $\lambda, \tilde{\lambda}, 4\lambda\tilde{\lambda} - \lambda'^2 \geq 0$. Expanding the scalar fields around the scalar potential minimum as $H = (\chi^+(v + h' + i\chi')/\sqrt{2})^T$ and $\Phi = (\tilde{v} + \phi' + i\eta')/\sqrt{2}$, the extended CP-even scalar mass matrix in the broken phase is

$$\mathcal{L} \supset -\frac{1}{2}\begin{pmatrix} h' & \phi' \end{pmatrix}\begin{pmatrix} 2\lambda v^2 & \lambda' v\tilde{v} \\ \lambda' v\tilde{v} & 2\tilde{\lambda}\tilde{v}^2 \end{pmatrix}\begin{pmatrix} h' \\ \phi' \end{pmatrix}. \quad (14)$$

We diagonalize it via the unitary rotation $h' = c_\phi h + s_\phi \phi$ and $\phi' = -s_\phi h + c_\phi \phi$, with $\tan 2\theta_\phi = \lambda' v\tilde{v}/(\tilde{\lambda}\tilde{v}^2 - \lambda v^2)$. The physical scalar masses are then related to the quartic couplings and VEVs as $(M_h M_\phi)^2 = (4\lambda\tilde{\lambda} - \lambda'^2)(v\tilde{v})^2$ and $M_h^2 + M_\phi^2 = 2(\lambda v^2 + \tilde{\lambda}\tilde{v}^2)$, and therefore λ and $\tilde{\lambda}$ can be expressed in terms of $M_h = 125.2$ GeV, $v = 246$ GeV,

[2]For the redefinitions of A_μ and Z'_μ, the leading-order terms are approximately accurate up to $\tilde{g}q' \lesssim 1$. However, for Z_μ, higher-order terms in the expansion, e.g., $\mathcal{O}(\epsilon_Z^3)$, become relevant for $\tilde{g}q' \gtrsim 10^{-2}$. On the other hand, the implied values of ϵ_A for $\tilde{g}q' \gtrsim 10^{-2}$ are excluded by searches for dark photons, as discussed in Sec. III B 1. Thus, we will only consider $\tilde{g}q' < 10^{-2}$ in this work, so that the leading-order terms in the field redefinitions remain dominant.

and inputs $\{M_\phi, \tilde{g}q', \lambda'\}$. The inequality $2\lambda' v\tilde{v} \leq |M_\phi^2 - M_h^2|$ is furthermore implied.

At one-loop order, λ' receives the RGE contributions $d\lambda'/d\ln\mu = -3(y_t y_T^t)^2/4\pi^2$, where we retain only the dominant box diagram expression. Fixing $\lambda'(\Lambda) = 0$ in the UV, the quartic coupling at scales below m_T can then be estimated, including threshold contributions, for $m_t \ll m_T$ as

$$\lambda' = \frac{3(y_t y_T^t)^2}{8\pi^2}\left[\ln\frac{\Lambda^2}{m_T^2} + 1\right], \tag{15}$$

which yields $\lambda' = 2 \times 10^{-2}(y_T^t/0.1)^2(L_T/55)$, assuming $y_t \approx \sqrt{2}m_t/v$. In this work, we will take $\lambda'(\Lambda) = 0$ at the scale $\Lambda = 10^{16}$ GeV and use the value of λ' generated by the running to low scales, rather than treating it as a free parameter. Consequently, in much of the relevant parameter space, it is not possible to satisfy the condition $2\lambda' v\tilde{v} \leq |M_\phi^2 - M_h^2|$ in the limit $M_\phi \ll M_h$. For simplicity, in the following we will therefore only consider the $M_\phi > M_h$ scenario.[3]

Another constraint on the scalar sector of the model arises from perturbative unitarity. The amplitudes for scattering processes $a \to b$ involving CP-even initial and final states $a, b \in \{W^+W^-, ZZ, h'h', \phi'\phi', Z'Z'\}$, can be decomposed into partial waves to build a coupled-channel matrix of $J = 0$ s-wave amplitudes,

$$a_0 = -\frac{1}{16\pi}\begin{Bmatrix} 4\lambda & \sqrt{2}\lambda & \sqrt{2}\lambda & 0 & 0 \\ \sqrt{2}\lambda & 3\lambda & \lambda & 0 & 0 \\ \sqrt{2}\lambda & \lambda & 3\lambda & \lambda'/2 & 0 \\ 0 & 0 & \lambda'/2 & 3\tilde{\lambda} & \tilde{\lambda} \\ 0 & 0 & 0 & \tilde{\lambda} & 3\tilde{\lambda} \end{Bmatrix}, \tag{16}$$

where initial/final state masses have been neglected and the limit of large s is taken. The condition $|\mathrm{Re}a_0| \leq 1/2$ for perturbative unitarity [48,49] is then applied to the largest eigenvalue of Eq. (16). If λ' is sufficiently small, the SM and $U(1)'$ sectors decouple and the subsequent bounds are $\lambda < 4\pi/3$ and $\tilde{\lambda} < 2\pi$. These upper bounds can be combined with the relations below Eq. (14) to derive an approximately allowed range of ϕ masses,

$$\frac{8\pi v^2}{3} + \frac{3(\lambda'\tilde{v})^2}{8\pi A} < M_\phi^2 < 4\pi\tilde{v}^2 + \frac{(\lambda' v)^2}{4\pi B}, \tag{17}$$

where $A = 1\text{–}3M_h^2/8\pi v^2$, $B = 1 - M_h^2/4\pi\tilde{v}^2$. The lower bound on M_ϕ is valid only for $\lambda' > 8\pi v A/3\tilde{v}$; otherwise, M_ϕ is compatible with perturbative unitarity down to the lower limit $M_\phi^2 \geq M_h^2 + 2\lambda' v\tilde{v}$. When the lower and upper limits coincide, no value of M_ϕ can satisfy the condition $|\mathrm{Re}a_0| \leq 1/2$. Solving this limit for λ' then indicates that $\lambda' < 4\pi \min[\tilde{v}B/v, \sqrt{2AB/3}] \approx 4\pi \min[\tilde{v}/v, \sqrt{2/3}]$ is required for perturbative unitarity in the scalar sector, where we neglected M_h in the second step. Finally, the lower bound $\tilde{v} > M_h/\sqrt{4\pi} \approx 35$ GeV is always satisfied for $M_\phi > M_h$, implying $\tilde{g}q' < 0.06$ for $M_{Z'} = 2.1$ GeV.

[3]Note that in the minimal model, $Z' \to \phi\phi$ decays, even if kinematically allowed, are forbidden by parity, and thus the presence of a light ϕ with $M_\phi \lesssim 1$ GeV would not change the main conclusions presented in Sec. II B.

B. Phenomenology in B decays

At scales relevant for B decays, couplings of Z' to down-type quarks are generated by one-loop diagrams such as in Fig. 2. The relevant effective Hamiltonian in the weak effective theory (WET) plus Z' is of the form

$$\mathcal{H}_{\rm eff} \supset C_{ij}^V \mathcal{O}_{ij}^V + C_{ij}^{\prime V}\mathcal{O}_{ij}^{\prime V} + \left[C_{ij}^T \mathcal{O}_{ij}^T + \mathrm{H.c.}\right], \tag{18}$$

where the vector and dipolelike operators are

$$\mathcal{O}_{ij}^{(\prime)V} = (\bar{d}_i \gamma_\mu P_{L(R)} d_j) Z'^\mu, \tag{19}$$

$$\mathcal{O}_{ij}^T = (\bar{d}_i \sigma_{\mu\nu} P_L d_j) Z'^{\mu\nu}, \tag{20}$$

respectively. The coefficients $C(\mu)$ can be matched to the full model at the electroweak scale, $\mu \sim M_W$, and then run down to $\mu \sim m_b$ under $SU(3)_c \times U(1)_{\rm em}$. The complete expressions for the coefficients $C(M_W)$ which we use in our numerical studies are provided in the Appendix.

It is instructive to understand important properties and limits of $C(\mu)$. First, the right-handed vector coupling vanishes identically, $C_{ij}^{\prime V}(M_W) = 0$. For $m_t \ll m_T$, the left-handed vector coupling at $\mu = M_W$ can be approximated as

$$C_{ij}^V(M_W) \approx \frac{1}{2}\mathcal{C}_{ij} m_t^2 \left[\tilde{g}q' s_R^2 X_t - \frac{g}{c_w}\Delta_{Z'} Y_t\right], \tag{21}$$

with $X_t = \ln m_T^2/M_W^2 - 1$, $Y_t \equiv Y(m_t^2/M_W^2) = 1.47$ using the function $Y(x)$ defined in the Appendix, and we define for convenience $\mathcal{C}_{ij} = 4G_F V_{ti}^* V_{tj}/16\sqrt{2}\pi^2$. The first term in Eq. (21) arises from the direct coupling of Z' to t/T in Eq. (11), while the second term is induced by the mixing of Z' into Z. The mixing of Z' into γ does not contribute,

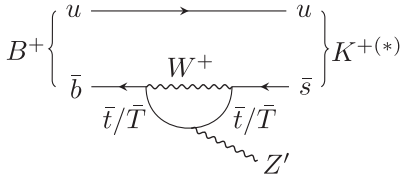

FIG. 2. Two-body decay contributing to $B^+ \to K^+ E_{\rm miss}$, with a single light Z' in the final state.

because the photon coupling to the FCNC down-type quark vector current vanishes due to gauge invariance. For $i = j$, the Z' also couples to down-type quarks according to Eq. (11). The expression in Eq. (21) only holds for $\tilde{g}q'$ sufficiently above the consistency bound in Eq. (5). To fit the Belle II excess in some of the parameter space, we find that $\tilde{g}q'$ is required to be close to the consistency bound. In this limit, the left-handed vector coupling is instead given by

$$C_{ij}^V(M_W) \approx \mathcal{C}_{ij} m_t m_T \tilde{g}q'. \tag{22}$$

The vector operators do not run under QED or QCD, so the expressions for C_{ij}^V and $C_{ij}^{\prime V}$ above and in the Appendix are also valid at $\mu \sim m_b$.

In the limit $m_t \ll m_T$, the dipolelike operator is given approximately at the matching scale $\mu = M_W$ by

$$C_{ij}^T(M_W) \approx m_i \mathcal{C}_{ij}\left[\tilde{g}q' s_R^2 A_t - e\epsilon_A B_t - \frac{g}{c_w}\Delta_{Z'} C_t\right], \tag{23}$$

where $A_t = 0.0323$, $B_t = 0.194$ and $C_t = 0.150$ are the numerical outputs of loop functions, given in the Appendix. Like the vector coupling C_{ij}^V, the first term in Eq. (23) is induced by Z' coupling directly to t/T. The second and third terms in Eq. (23) are generated by the mixing of Z' into γ and Z, respectively. The running of C_{ij}^T down to $\mu \sim m_b$ is dominated by QCD corrections. However, a detailed treatment of the running is not necessary for the following analysis, as we will demonstrate shortly.

Through these vector and dipolelike interactions, the Z' can be produced on shell in the process $B^+ \to K^+ Z'$ for $M_{Z'} < m_B - m_K$, with the branching fraction

$$\mathcal{B}(B^+ \to K^+ Z') = \tau_{B^+} \frac{|\vec{p}_K|^3}{8\pi M_{Z'}^2}\left|C_{\mathrm{bs}}^V f_+ + C_{\mathrm{bs}}^T \tilde{f}_T\right|^2, \tag{24}$$

where τ_{B^+} is the B^+ lifetime, $\vec{p}_K$ is the three-momentum of K^+ in the B^+ rest frame, and $\tilde{f}_T = 2M_{Z'}^2 f_T/(m_B + m_K)$. Here, f_+ and f_T are the vector and tensor $B \to K$ transition form factors evaluated at the squared momentum transfer $q^2 = M_{Z'}^2$, respectively. We note that the coupling C_{sb}^T also contributes to the process, but is suppressed by m_s/m_b with respect to C_{bs}^T and is therefore neglected. The Z' can also be produced on shell in the process $B \to K^* Z'$ for $M_{Z'} < m_B - m_{K^*}$, with

$$\mathcal{B}(B \to K^* Z') = \tau_B \frac{|\vec{p}_{K^*}|}{4\pi}\left\{\left|C_{\mathrm{bs}}^V \tilde{V} - C_{\mathrm{bs}}^T \tilde{T}_1\right|^2 + \left|C_{\mathrm{bs}}^V \tilde{A}_1 - C_{\mathrm{bs}}^T \tilde{T}_2\right|^2 + 8\left|C_{\mathrm{bs}}^V \tilde{A}_{12} - C_{\mathrm{bs}}^T \tilde{T}_{23}\right|^2\right\}, \tag{25}$$

where we define

$$\tilde{V} = \frac{|\vec{p}_{K^*}|}{m_B + m_{K^*}} V, \qquad \tilde{T}_1 = 2|\vec{p}_{K^*}| T_1,$$
$$\tilde{A}_1 = \frac{m_B + m_{K^*}}{2m_B} A_1, \qquad \tilde{T}_2 = \frac{m_B^2 - m_{K^*}^2}{m_B} T_2,$$
$$\tilde{A}_{12} = \frac{m_{K^*}}{M_{Z'}} A_{12}, \qquad \tilde{T}_{23} = \frac{M_{Z'} m_{K^*}}{m_B + m_{K^*}} T_{23}. \tag{26}$$

Here, V, A_1, A_{12}, T_1, T_2 and T_{23} are vector, axial-vector and tensor $B \to K^*$ transition form factors, respectively, evaluated at $q^2 = M_{Z'}^2$. The first two terms and the last term in Eq. (25) contribute to transversely and longitudinally polarised K^* in the final state, respectively. In this work, we use the Bharucha-Straub-Zwicky [50] parametrization fit results of Ref. [51] for the form factors in Eqs. (24) and (25).

In order to contribute to the observed excess in $B^+ \to K^+ E_{\mathrm{miss}}$, the Z' must decay outside the Belle II detector or to invisible final states. This occurs with the probability

$$P_{\mathrm{inv}} = P_{\mathrm{out}} + (1 - P_{\mathrm{out}})\mathcal{B}(Z' \to \mathrm{inv}), \tag{27}$$

where $P_{\mathrm{out}} = \exp(-L/L_{Z'})$ and $L_{Z'} = \beta\gamma\tau_{Z'} = \beta\gamma/\Gamma_{Z'}$. Here, $\Gamma_{Z'}$ is the total decay width of Z', $\mathcal{B}(Z' \to \mathrm{inv})$ is the invisible Z' branching fraction, $L \approx 5$ m is the distance from the interaction point to the edge of the Belle II detector, and $\beta\gamma$ is the boost of Z' in the lab frame. The boost can be estimated to lie in the range $\beta\gamma \in [0.6, 1.6]$ for $M_{Z'} = 2.1$ GeV and the incoming e^+e^- energies at SuperKEKB [52].

The Z' decay width and invisible branching fraction are determined in the minimal model as follows: the total width of Z' is $\Gamma_{Z'} = 3\Gamma_{\nu\bar{\nu}} + \Gamma_{e^+e^-} + \Gamma_{\mu^+\mu^-} + \Gamma_{\mathrm{hadr}}$, where the Z' decays to SM fermions via the kinetic and mass mixing, as shown in Fig. 3 (left), have the decay rate

$$\Gamma_{f_i \bar{f}_j} = \frac{M_{Z'}}{12\pi}[(v_{Z'}^f)^2 + (a_{Z'}^f)^2]_{ij}, \tag{28}$$

where $v_{Z'}^f$ and $a_{Z'}^f$ are given in Eq. (11), and we neglect final-state masses. For $M_{Z'} = 2.1$ GeV, the approximation is valid for $f = \nu$, e, μ. For $M_{Z'}$ sufficiently above the regime of nonperturbative QCD and away from known hadronic thresholds, quark-hadron duality can be used to estimate the inclusive hadronic decay rate as

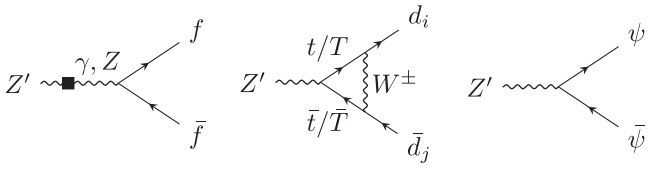

FIG. 3. Left and center: one-loop induced decays of the light Z' in the minimal model. Right: tree-level decay of Z' to a vectorlike dark fermion ψ, considered in Sec. III.

$$\Gamma_{\rm hadr} = N_c \left(1 + \frac{\Delta_V}{\pi}\right) \left[\Theta_{uu}\Gamma_{u\bar{u}} + \sum_{d_i,d_j=d,s} \Theta_{d_i d_j}\Gamma_{d_i\bar{d}_j}\right], \quad (29)$$

where $N_c = 3$ and $\Delta_V = \alpha_s + 0.522\alpha_s^2 - 1.04\alpha_s^3 - 3.45\alpha_s^4$ accounts for perturbative QCD corrections [53–55], with $\alpha_s(M_{Z'}) = 0.297$ and $n_f = 3$ quark flavors. Down-type quark contributions to the inclusive hadronic decay rate are also generated by the vector coupling C_{ij}^V and dipolelike coupling C_{ij}^T, as shown in Fig. 3 (center). The former can be included by replacing $[v_{Z'}^d]_{ij} \to [v_{Z'}^d]_{ij} + C_{ij}^V/2$ and $[a_{Z'}^d]_{ij} \to [a_{Z'}^d]_{ij} + C_{ij}^V/2$ in Eq. (28), while the latter contribution is proportional to the light quark masses and is therefore neglected. We include the kinematical factors Θ in Eq. (29), where $\Theta_{ij}^2 = 1 - (m_{P_i} + m_{P_j})^2/M_{Z'}^2$, to approximate the suppression of the decay rate due to the lightest hadronic thresholds ($Z' \to \pi\pi, \pi K, KK$), where $m_{P_i} = m_\pi$ is taken for $i = u, d$ and $m_{P_i} = m_K$ for $i = s$. We note that the applicability of this approach for $M_{Z'} = 2.1$ GeV is marginal, but nevertheless sufficient for our purposes, as explained in more detail later in this section and in Sec. III.[4]

Only $Z' \to \nu\bar{\nu}$ can contribute to invisible Z' decays in the minimal model, assuming that the other decay modes ($Z' \to e^+e^-/\mu^+\mu^-$/hadr) are visible at Belle II (in the central drift chamber, electromagnetic calorimeter or K_L–muon detector), yielding the invisible branching fraction $\mathcal{B}(Z' \to \text{inv}) = 3\Gamma_{\nu\bar{\nu}}/\Gamma_{Z'}$. The contribution of Z' to the $B^+ \to K^+ E_{\rm miss}$ rate is then

$$\mathcal{B}(B^+ \to K^+ E_{\rm miss}) = \int dq^2 \frac{d\mathcal{B}(B^+ \to K^+\nu\bar{\nu})|_{\rm SM}}{dq^2} + \mathcal{B}(B^+ \to K^+ Z')P_{\rm inv}, \quad (30)$$

where the factorization of the second term holds in the narrow width approximation of Z'. The narrow width of Z' also makes it safe to neglect the interference between the SM and $B^+ \to K^+(Z' \to)\nu\bar{\nu}$.

In Ref. [1], the Belle II inclusive tagging analysis (ITA) search for $B^+ \to K^+\nu\bar{\nu}$ observed an excess of events at the reconstructed momentum transfer $q^2_{\rm rec} \sim 4$ GeV^2. If the missing energy excess is interpreted as neutrinos (SM) plus the contribution of an undetected Z' in the final state, $B^+ \to K^+ Z'$, the ITA $q^2_{\rm rec}$ spectrum data provide the best-fit mass $M_{Z'} = (2.1 \pm 0.1)$ GeV [2,4]. The excess can then be interpreted as the presence of a vector and/or dipolelike coupling of the Z' to the $b \to s$ transition. In Refs. [2,4], we considered the presence of one of these couplings at a time, performing a fit to the Belle II data to find the best-fit coupling and therefore the implied size of $\mathcal{B}(B^+ \to K^+ Z')$ in each case. As both couplings also contribute to the process $B \to K^* Z'$, the fit in Refs. [2,4] also included the *BABAR* q^2 data used to derive an upper bound on $B^0 \to K^{*0}\nu\bar{\nu}$ [60].[5]

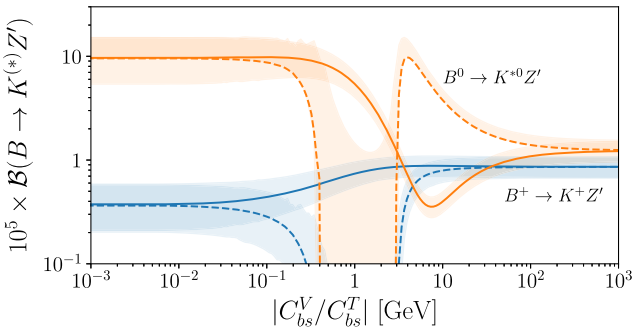

FIG. 4. Favored branching fractions for $B^+ \to K^+ Z'$ and $B^0 \to K^{*0} Z'$ from the Belle II [1] and *BABAR* [60] data, as a function of the ratio $|C_{\rm bs}^V/C_{\rm bs}^T|$ for $M_{Z'} = 2.1$ GeV. Solid (dashed) lines show positive (negative) values of $C_{\rm bs}^V/C_{\rm bs}^T$.

Here, assuming that both the vector and dipolelike couplings are nonzero, we perform a fit to the Belle II and *BABAR* q^2 data for $M_{Z'} = 2.1$ GeV, but now vary the ratio $r_c \equiv C_{\rm bs}^V/C_{\rm bs}^T$. From the fit, we obtain the expected branching fractions for $B^+ \to K^+ Z'$ and $B^0 \to K^{*0} Z'$ shown in Fig. 4. Firstly, when the vector or dipolelike coupling dominates, which occurs when r_c is much above or below $\tilde{f}_T/f_+ \approx 1.5$ GeV, respectively, we recover the results of Ref. [2,4], i.e.,

$$\frac{\mathcal{B}(B^+ \to K^+ Z')|_{\rm exp}}{10^{-6}} = \begin{cases} 8.6^{+2.1}_{-1.9} & |r_c| \gg \tilde{f}_T/f_+ \\ 3.7^{+2.1}_{-1.6} & |r_c| \ll \tilde{f}_T/f_+ \end{cases}, \quad (31)$$

which can be seen to the far right and left of Fig. 4. For a dominant dipolelike coupling, a smaller $\mathcal{B}(B^+ \to K^+ Z')$ provides a better fit to the *BABAR* q^2 data, because $C_{\rm bs}^T$ contributes more to $B^0 \to K^{*0} Z'$ than $C_{\rm bs}^V$. Explicitly,

$$\frac{\mathcal{B}(B^0 \to K^{*0} Z')}{\mathcal{B}(B^+ \to K^+ Z')} = \begin{cases} 1.43 & |r_c| \gg \tilde{f}_T/f_+ \\ 26.0 & |r_c| \ll \tilde{f}_T/f_+ \end{cases}. \quad (32)$$

For intermediate values of r_c, interference effects become important and depend on the sign of r_c. In Fig. 4, the solid (dashed) lines illustrate the fit results for positive (negative) values of r_c. For $r_c < 0$, the terms in Eq. (24) contributing to $B^+ \to K^+ Z'$ can interfere destructively, and for

[4]A data-driven approach using $e^+e^- \to$ hadrons and hadronic τ decay data would be necessary for $M_{Z'} \lesssim 2$ GeV to account for the effects of vector and axial-vector meson resonances (ρ, ω, ϕ, and f_1), as performed in Refs. [56–59].

[5]Very recently, Belle II published the results of their first search for inclusive $B \to X_s\nu\bar{\nu}$ decays [61] using a sum over exclusive states. However their derived upper bound on $\mathcal{B}(B \to X_s\nu\bar{\nu}) < 3.2 \times 10^{-4}$ is not competitive with existing constraints targeting individual exclusive decay modes.

$-3 \lesssim r_c/\text{GeV} \lesssim -0.04$, it is no longer possible to address the Belle II excess and be compatible with the *BABAR* q^2 data. For $r_c > 0$, destructive interference may instead occur in $\mathcal{B}(B^0 \to K^{*0} Z')$, which can be seen for $4 \lesssim r_c/\text{GeV} \lesssim 20$ in Fig. 4.

For the minimal aligned $U(1)'$ model to accommodate the Belle II excess, it must satisfy

$$\mathcal{B}(B^+ \to K^+ Z') P_{\text{inv}} = \mathcal{B}(B^+ \to K^+ Z')|_{\text{exp}}, \quad (33)$$

where the lhs is the model prediction and the rhs is the best-fit branching fraction from the Belle II and *BABAR* q^2 data. However, we find that when the combination $|C_{\text{bs}}^V f_+ + C_{\text{bs}}^T \tilde{f}_T|$ in Eq. (24) is large enough to saturate Eq. (33), the vector coupling always dominates over the dipolelike coupling. Specifically, C_{bs}^V is determined at the scale $\mu = M_W$ predominantly by the direct coupling of Z' to t/T and C_{bs}^T by the $\gamma - Z'$ mixing. The ratio of couplings is then given at $\mu = M_W$ by

$$\frac{|r_c|}{\text{GeV}} \approx 2 \times 10^4 \left[\frac{y_T^t}{0.1}\right]^2 \left[\frac{\text{TeV}}{m_T}\right]^2 \left[\frac{10^{-3}}{\tilde{g} q'}\right]^2 \left[\frac{X_t/L_T}{0.07}\right]. \quad (34)$$

Running under QCD to $\mu \sim m_b$ is expected to modify the numerical size of the dipolelike coupling at most by a factor of a few, and thus the large hierarchy between the couplings as expressed in Eq. (34) remains valid at $\mu \sim m_b$. In Eq. (33), we therefore neglect the dipolelike coupling and use the best-fit branching fraction in the limit $|r_c| \gg \tilde{f}_T/f_+$, which is equivalent to requiring $|C_{\text{bs}}^V|^2 P_{\text{inv}} = |C_{\text{bs}}^V|^2|_{\text{exp}}$ with the best-fit vector coupling $C_{\text{bs}}^V|_{\text{exp}} = (1.4 \pm 0.5) \times 10^{-8}$ [2].

In Fig. 5, we investigate the properties of Z' if Eq. (33) is satisfied and $B^+ \to K^+ (Z' \to) \nu\bar{\nu}$ therefore provides the excess in missing energy at Belle II. In the top panel, we show the branching fractions of Z' as a function of m_T for $y_T^t = 1$. The solid (dashed) lines show the choice of the kinetic mixing at the high scale $\epsilon_B(\Lambda) = 0$ (10^{-4}), while the bands indicate the $\pm 1\sigma$ uncertainty from the best-fit branching fraction in Eq. (33). We show the inclusive hadronic branching fraction $Z' \to$ hadr and its contributions from different light quark flavors ($\Gamma_{u\bar{u}/d\bar{d}/s\bar{s}}$ induced by $\epsilon_{A,Z}$ and δ_Z dominate, while $\Gamma_{d\bar{s}/s\bar{d}}$ from C_{ij}^V are negligible) and the leptonic branching fractions $Z' \to \nu\bar{\nu}/e^+e^-/\mu^+\mu^-$. We note that for $y_T^t = 1$, it is not possible to satisfy Eq. (33) for $m_T \lesssim 300$ GeV, due to the suppression of $\mathcal{B}(Z' \to \nu\bar{\nu})$, which we indicate as a dark gray region. The observed branching fractions follow purely from the behavior of the kinetic and mass mixing. For $m_T \lesssim 10$ TeV, $\epsilon_A \gg \Delta_{Z'}$ and Z' behaves like a dark photon with severely suppressed couplings to SM neutrinos in both $\epsilon_B(\Lambda) = 0$ (10^{-4}) scenarios. For $\epsilon_B(\Lambda) = 0$ and $m_T \gtrsim 10$ TeV, $\epsilon_Z \ll \tilde{\delta}_A$ and Z' has SM Z-like branching fractions. In this limit, $\mathcal{B}(Z' \to \nu\bar{\nu}) = 0.29$. On the other hand, in the $\epsilon_B(\Lambda) = 10^{-4}$ scenario, the additional contribution to ϵ_A suppresses the branching fractions to neutrinos in the whole considered m_T range. When $m_T \gtrsim 200$ TeV (50 TeV), the Yukawa coupling y_t violates perturbative unitarity for $\epsilon_B(\Lambda) = 0$ (10^{-4}), indicated as a vertical green dashed line and shaded (unshaded) region. Direct experimental probes of y_t discussed in Sec. III B 2 represent even stronger constraints. Finally, note that for any given value of m_T there is a (fine-tuned) value of $\epsilon_B(\Lambda)$ that exactly cancels the value of ϵ_A induced by the running, leading to the Z' branching fractions that are SM Z-like. In the following, we do not consider such fine-tuned solutions.

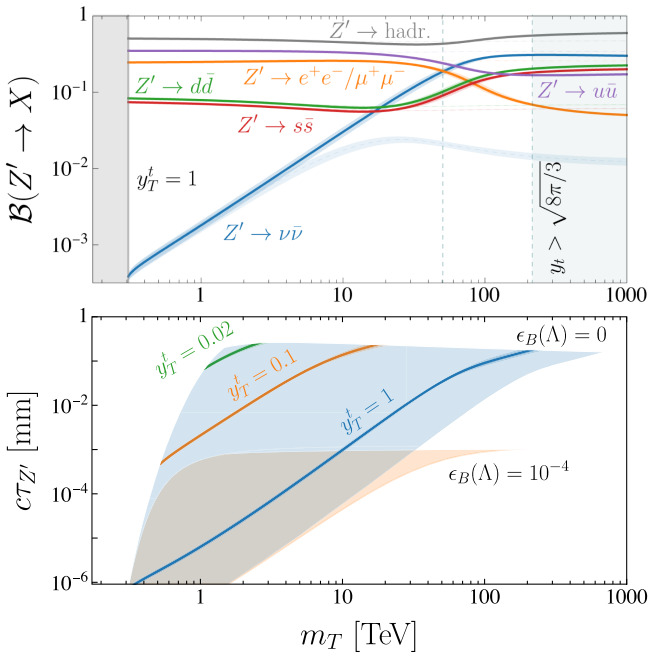

FIG. 5. Top: branching fractions of Z' in the minimal model accommodating the Belle II measurement in Eq. (33) as a function of m_T, for $y_T^t = 1$. Solid (faint dashed) lines are shown for $\epsilon_B(\Lambda) = 0$ (10^{-4}). Also shown are y_t perturbativity limits (vertical dashed lines) for both cases. Bottom: proper lifetime of Z' as a function of m_T for $\epsilon_B(\Lambda) = 0$ and different values of y_T^t. Envelopes of possible $c\tau_{Z'}$ values are shown for $\epsilon_B(\Lambda) = 0$ and 10^{-4}.

In the bottom panel of Fig. 5, we instead show the expected proper lifetime of Z' ($c\tau_{Z'}$) as a function of m_T, for $\epsilon_B(\Lambda) = 0$ and three y_T^t values. The blue (orange) envelopes illustrate the total range of possible $c\tau_{Z'}$ values for $\epsilon_B(\Lambda) = 0$ (10^{-4}); the upper and lower edges correspond to the maximum values of y_t and y_T^t compatible with perturbative unitarity, respectively. On the left edges of the envelopes, the Belle II data cannot be satisfied due to the suppression of $\mathcal{B}(Z' \to \nu\bar{\nu})$. In general, it can be seen that the lifetime of Z' cannot exceed $c\tau_{Z'} \sim 0.3$ mm, because the lifetime is maximized when the irreducible mass mixing dominates the interactions of Z'. For larger $\epsilon_B(\Lambda)$, in the

absence of fine-tuning, Z' is more dark photonlike and decays faster. For the expected boosts at Belle II, we conclude that the probability of Z' decaying outside the detector is negligible, so $P_{\rm inv} \approx \mathcal{B}(Z' \to \nu\bar{\nu})$. Thus, the effective size of the Belle II detector, $L \approx 5$ m, has no impact on the results.

Finally, we note that the consistency condition in Eq. (5) implies that there is a minimum value of y_T^t which is compatible with the Belle II data. If Eq. (5) is saturated, the vector coupling $C_{\rm bs}^V$ is given by Eq. (22). In this limit, $|C_{\rm bs}^V|^2 P_{\rm inv} = |C_{\rm bs}^V|^2_{\rm exp}$ can be rearranged for y_T^t, giving

$$y_T^t \gtrsim \frac{\sqrt{2} C_{\rm bs}^V|_{\rm exp}}{m_t M_{Z'} \mathcal{C}_{\rm bs} \sqrt{P_{\rm inv}}} \approx 0.012 \left[\frac{0.29}{P_{\rm inv}}\right]^{1/2}, \qquad (35)$$

for $m_t \ll m_T$, $\epsilon_B(\Lambda) = 0$, and $P_{\rm inv}$ evaluated at the consistency limit of Eq. (5). In the minimal model, the Z' interactions are SM Z-like in this regime, and thus $P_{\rm inv} = 0.29$. The lower bound on y_T^t can be seen visually in Fig. 5 in the top left corner of the $c\tau_{Z'}$ envelope for $\epsilon_B(\Lambda) = 0$. Using Eq. (5), it is also possible to derive a lower bound on the gauge coupling, $\tilde{g} q' \gtrsim C_{\rm bs}^V|_{\rm exp} / \mathcal{C}_{\rm bs} m_t m_t \sqrt{P_{\rm inv}}$.

In the top panel of Fig. 5, it can be seen that the Z' also has sizeable branching fractions to $e^+e^-/\mu^+\mu^-$ in both the dark photon and SM Z-like limits. Stringent constraints therefore apply from measurements of $B \to K^{(*)}\ell^+\ell^-$, with $\ell = e, \mu$ being either prompt or displaced depending on the value of $c\tau_{Z'}$. For prompt $Z' \to e^+e^-/\mu^+\mu^-$ decays, the Z' will appear as a peak of events in the $[q_i^2, q_j^2]$ bin around $q^2 = M_{Z'}^2$ [62,63]. On the other hand, dedicated LHCb searches for B decays to resonant displaced dimuons provide even stronger bounds on the process $B \to K^{(*)}(Z' \to)\mu^+\mu^-$ [44,45]. For Z' lifetimes in the range $c\tau_{Z'} \in [0.03, 300]$ mm, the searches place an upper limit on $\mathcal{B}(B \to K^{(*)}Z')\mathcal{B}_{\mu^+\mu^-}$, with $\mathcal{B}_{\mu^+\mu^-} = \mathcal{B}(Z' \to \mu^+\mu^-)$. However, even for $c\tau_{Z'} < 0.03$ mm, when the Z' decays within the decay time resolution of the experiment, the limits for $c\tau_{Z'} = 0.03$ mm remain applicable.

In Fig. 6, we demonstrate how the LHCb constraints exclude the minimal $U(1)'$ model as an explanation of the Belle II excess. The black solid (dashed) line shows the 95% CL upper bound on the $B \to K^{(*)}(Z' \to)\mu^+\mu^-$ branching fraction from LHCb. The blue region shows the expected range of $\mathcal{B}(B \to K^{(*)}Z')\mathcal{B}_{\mu^+\mu^-}$ values if the Belle II data are accommodated, for $\epsilon_B(\Lambda) = 0$. The observed upper limit and expected branching fraction of the $B^0 \to K^{*0}$ mode are rescaled by the ratio in Eq. (32) in the limit $|r_c| \gg \tilde{f}_T/f_+$, so that the expected branching fractions of the $B^+ \to K^+$ and $B^0 \to K^{*0}$ modes coincide in the figure. It is evident that the LHCb data exclude all of the viable parameter space of the minimal model. Furthermore, different values of $\epsilon_B(\Lambda)$ do not change this conclusion;

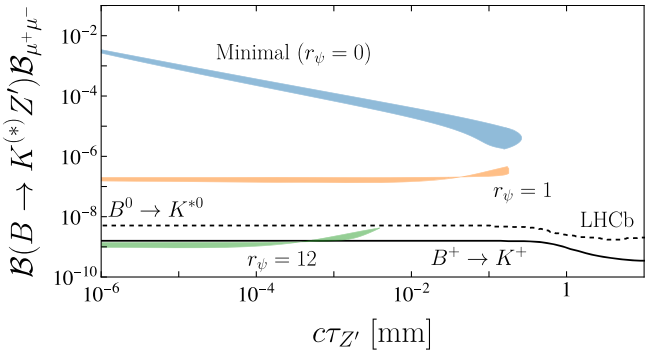

FIG. 6. Branching fractions of $B \to K^{(*)}(Z' \to)\mu^+\mu^-$ in the model with a vectorlike dark fermion ψ (for two values of the $U(1)'$ charge ratio r_ψ) which accommodate the Belle II data, compared to the LHCb upper limits (black, solid for $B \to K$ and dashed for $B \to K^*$). See text for details.

even if fine-tuning suppresses ϵ_A, the Z' still decays with a large branching fraction to $Z' \to \mu^+\mu^-$ via the mass mixing.[6]

We briefly return to the method used to estimate the inclusive hadronic decay rate in Eq. (29). Uncertainties from the use of perturbative QCD corrections instead of the data-driven approach enter the estimate of the total Z' width and therefore all Z' branching fractions. While these uncertainties may result in small changes to the results presented in Figs. 5 and 6, the decisive exclusion of the model by LHCb makes the study of such uncertainties unnecessary.

To finish this section, we conclude that in order for the $U(1)'$ gauge boson Z', coupled to the top partner T', to provide the missing energy signature and evade the LHCb bounds, it must decay invisibly to additional light, non-SM states. It is plausible that there are SM-singlet fields charged under the $U(1)'$. Such feebly interacting states would naturally evade detection and could make up an extended dark sector. In Sec. III, we consider the scenario of a single vectorlike dark fermion ψ with a $U(1)'$ charge. First, we review how this addition changes the phenomenology at Belle II, and explore how other experimental probes (in addition to LHCb) constrain the parameter space. In this setup, we then explore the interesting possibility of ψ being some or all of the DM.

III. MODEL WITH DARK FERMION

Here we extend the minimal model of Sec. II, by introducing a SM-singlet vectorlike dark fermion $\psi(\mathbf{1}, \mathbf{1}, 0, q'_\psi)$ which we allow to have a different $U(1)'$

[6]This bound could thus also be important for the gauged $U(1)_{B_3-L_3}$ model proposed in Ref. [18], even though the Z' width is dominated by the tree-level mediated $Z' \to \nu_\tau\bar{\nu}_\tau$, as well as for the models presented in Ref. [26].

charge (q'_ψ) compared to T' and Φ. The Lagrangian now includes

$$\mathcal{L} \supset \bar{\psi}(i\not{D} - m_\psi)\psi. \tag{36}$$

The dark fermion ψ interacts with Z' and Z according to Eqs. (11) and (13), respectively, with $\mathfrak{v}^\psi = q'_\psi$, $\mathfrak{a}^\psi = 0$. There are two additional free parameters with respect to the minimal $U(1)'$ model: the vectorlike mass m_ψ and the $U(1)'$ charge ratio $r_\psi = q'_\psi/q'$.

A. Phenomenology in B decays

At Belle II, the production of Z' with $M_{Z'} = 2.1$ GeV is the same as described in Sec. II, i.e., $B^+ \to K^+ Z'$ in Fig. 2. For $2m_\psi > M_{Z'}$, the Z' cannot decay at tree level via $Z' \to \psi\bar{\psi}$ (shown in Fig. 3, right) and the discussion is identical to Sec. II. For $2m_\psi < M_{Z'}$ on the other hand, $Z' \to \psi\bar{\psi}$ becomes kinematically allowed and the total decay width is given by $\Gamma_{Z'} = 3\Gamma_{\nu\bar{\nu}} + \Gamma_{e^+e^-} + \Gamma_{\mu^+\mu^-} + \Gamma_{\text{hadr}} + \Gamma_{\psi\bar{\psi}}$, with the decay rate for $Z' \to \psi\bar{\psi}$, as follows:

$$\Gamma_{\psi\bar{\psi}} = \frac{M_{Z'}}{12\pi} f_\psi (\tilde{g} q'_\psi)^2. \tag{37}$$

Here, $f_\psi = f(m_\psi^2/M_{Z'}^2)$ with $f(x) = (1+2x)\sqrt{1-4x}$. In addition to the three neutrino final states, $Z' \to \psi\bar{\psi}$ also contributes to the total invisible branching fraction as $\mathcal{B}(Z' \to \text{inv}) = (3\Gamma_{\nu\bar{\nu}} + \Gamma_{\psi\bar{\psi}})/\Gamma_{Z'}$.

We now repeat the exercise of the previous section and determine where Eq. (33) holds, and therefore the Belle II excess is accommodated in the extended model. We furthermore examine the properties of Z', T and ψ in the viable parameter space. For simplicity in the following we restrict our discussion to the limit $\epsilon_B(\Lambda) = 0$. Firstly, in the top panel of Fig. 7, we show the Z' branching fractions as a function of m_T for $y_T^t = 0.1$, $m_\psi = 1$ GeV and $r_\psi = 1$. We first note the dominance of the decay mode $Z' \to \psi\bar{\psi}$ for $m_T \lesssim 7$ TeV. In this regime, the Z' is again dark photonlike, with $Z' \to \psi\bar{\psi}$ making up for the shortfall in $Z' \to \nu\bar{\nu}$ and the other decay modes being suppressed with respect to Fig. 5. As r_ψ is increased, the other decay modes are further suppressed relative to $Z' \to \psi\bar{\psi}$. For $m_T \gtrsim 7$ TeV, the branching fractions again tend towards the SM Z-like limit. Eventually, however, for $m_T \gtrsim 30$ TeV, the Yukawa coupling y_t violates perturbative unitarity. In the bottom panel of Fig. 7, we instead show $c\tau_{Z'}$ as a function of m_T for $m_\psi = 1$ GeV, $r_\psi = 1$, and three values of y_T^t. The blue (orange) envelope shows the total range of possible $c\tau_{Z'}$ values for $r_\psi = 1$ (12). The presence of $Z' \to \psi\bar{\psi}$ extends the range of possible $c\tau_{Z'}$ values with respect to Fig. 5. Larger values of r_ψ increase the partial decay rate for $Z' \to \psi\bar{\psi}$ and therefore decrease the maximum $c\tau_{Z'}$. For $r_\psi \ll 1$, the Z' branching fractions and lifetime tend towards those shown in Fig. 5. Again,

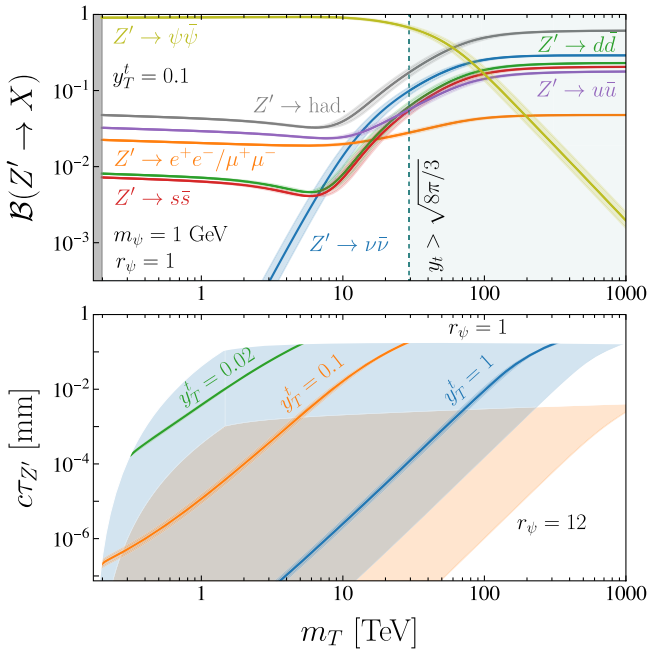

FIG. 7. As in Fig. 5, but with branching fractions (top) and the proper lifetime (bottom) of Z' in the model with a dark fermion ψ, for $y_T^t = 0.1$, $m_\psi = 1$ GeV and $r_\psi = 1$. The envelope of possible $c\tau_{Z'}$ values is also shown for $r_\psi = 12$.

$c\tau_{Z'} \sim 0.3$ mm presents an absolute maximum possible lifetime of Z'.

With these results, we can return to whether the model is compatible with the displaced $B \to K^{(*)}(Z' \to)\mu^+\mu^-$ LHCb bounds. In the top panel of Fig. 7, it can be seen that the $Z' \to \mu^+\mu^-$ branching fraction remains appreciable for $r_\psi = 1$. Thus, the $U(1)'$ charge ratio r_ψ must be large enough for $\mathcal{B}_{\mu^+\mu^-}$ to be sufficiently suppressed. In Fig. 6, we show as orange and green regions the expected range of $\mathcal{B}(B \to K^{(*)}Z')\mathcal{B}_{\mu^+\mu^-}$ values for $r_\psi = 1$ and 12, respectively. Comparing to the 95% CL upper limits, the $r_\psi = 1$ scenario is excluded, while $r_\psi = 12$ evades the $B \to K$ constraint for sufficiently small $c\tau_{Z'}$. An estimate of the required r_ψ can be found using $\mathcal{B}_{\mu^+\mu^-} \ll 1$ when $\mathcal{B}(Z' \to \psi\bar{\psi}) \approx 1$ and the other Z' decay modes are dark photonlike but suppressed. This also applies to the inclusive hadronic decay modes, making the impact of uncertainties from the use of perturbative QCD estimates negligible. Then, Eqs. (24), (28), and (37) can be combined to find that

$$r_\psi \gtrsim 10.1 \left[\frac{0.44}{f_\psi}\right]^{1/2} \left[\frac{L_T}{55}\right], \tag{38}$$

must be satisfied to evade the LHCb bounds. Note that the relatively large charge ratio required can also be accommodated by introducing several dark fermions with $\mathcal{O}(1)$ charge ratios. We briefly comment on this and other possible model extensions in Sec. IV.

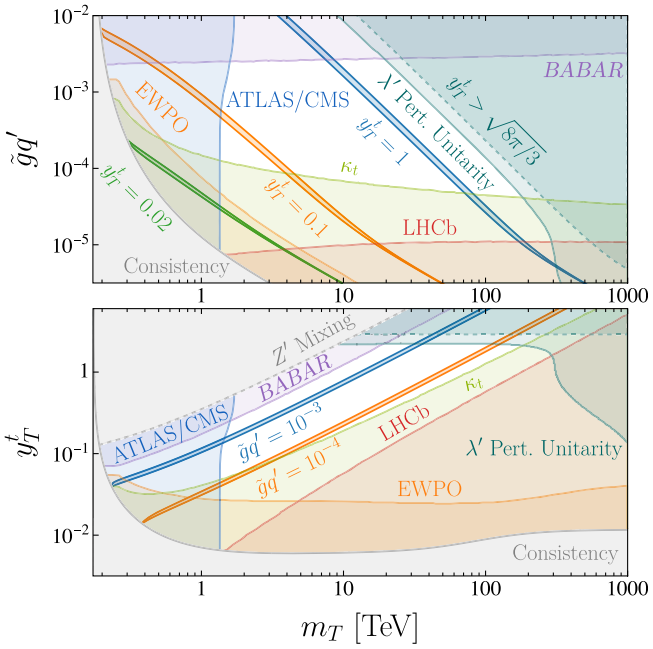

FIG. 8. Top: allowed and excluded regions in the $(m_T, \tilde{g}q')$ plane for the $U(1)'$ charge ratio $r_\psi = 12$ and vectorlike dark fermion mass $m_\psi = 1$ GeV. The Belle II excess can be accommodated anywhere above the *Consistency* region (in gray), with the blue, orange, and green bands indicating the favored regions for fixed y_T^t. Other constraints originate from dark photon searches at *BABAR* (purple), collider searches for top partners at ATLAS/CMS (blue), the measurements of the top Yukawa coupling (κ_t, light green), LHCb search for $B \to K^{(*)}(Z' \to \mu^+\mu^-)$ (red), EWPO (orange), and perturbative unitarity (dark green). Bottom: the same constraints, but in the (m_T, y_T^t) plane. The Belle II favored regions are shown as blue and orange bands for two fixed values of $\tilde{g}q'$. See text for details.

As the model is not ruled out by LHCb for $r_\psi \gtrsim 10$, we now examine other constraints on the model, which will be summarized in Sec. III B. In Fig. 8, we show the most stringent bounds in the $(m_T, \tilde{g}q')$ plane (top panel) and (m_T, y_T^t) plane (bottom panel), for the benchmark parameters $r_\psi = 12$ and $m_\psi = 1$ GeV. The Belle II excess can be accommodated anywhere above the gray region labeled *Consistency*, which is inaccessible as it violates the consistency condition in Eq. (5). On the other hand, the value of y_T^t needed to explain the Belle II data eventually violates perturbative unitarity for $y_T^t > \sqrt{8\pi/3}$, which we show as a dark green dashed line. We also show the regions of the parameter space which are favored by the Belle II data for specific values of y_T^t (top panel) and $\tilde{g}q'$ (bottom panel), with the bands indicating the $\pm 1\sigma$ uncertainty on $C_{\rm bs}^V|_{\rm exp}$. For $\tilde{g}q'$ well above the consistency bound in Eq. (5), an estimate of the favored region can be obtained by rearranging $|C_{\rm bs}^V|^2 P_{\rm inv} = |C_{\rm bs}^V|^2|_{\rm exp}$ using Eq. (21) (neglecting the contribution from $Z - Z'$ mixing) and $P_{\rm inv} \approx \mathcal{B}(Z' \to \psi\bar{\psi}) \approx 1$, to find

$$\tilde{g}q' \approx \frac{\mathcal{C}_{\rm bs}}{C_{\rm bs}^V|_{\rm exp}} \left(\frac{m_t M_{Z'} y_T^t}{2 m_T}\right)^2 X_t \approx 1.2 \times 10^{-3} \left[\frac{y_T^t}{0.5}\right]^2 \left[\frac{10\ \text{TeV}}{m_T}\right]^2 \left[\frac{X_t}{8.6}\right]. \quad (39)$$

As $\tilde{g}q'$ approaches the consistency bound, the scaling changes to $\tilde{g}q' \approx M_{Z'} y_T^t / \sqrt{2} m_T$. On the other hand, this regime is excluded by the other existing experimental constraints. The region not yet excluded thus lies between $1.3 \lesssim m_T/\text{TeV} \lesssim 170$ and $4 \times 10^{-5} \lesssim \tilde{g}q' \lesssim 3 \times 10^{-3}$. Converted to the VEV of Φ, we then find that the Belle II excess can be viably explained for $0.8 \lesssim \tilde{v}/\text{TeV} \lesssim 48$.

Before summarizing the experimental bounds on the model in the next section, we describe the remaining theoretical bounds shown in Fig. 8. The parameter space where perturbative unitarity is violated by the quartic coupling λ' in Eq. (15) is shown as a dark green shaded region. This boundary of the allowed region in Fig. 8 is given by the approximate condition

$$\tilde{g}q' \lesssim 8.6 \times 10^{-3} \left[\frac{10\ \text{TeV}}{m_T}\right]^2 \left[\frac{55}{L_T}\right] \left[\frac{X_t}{8.6}\right]^2. \quad (40)$$

In the (m_T, y_T^t) plane, we do not show the parameter space in the top left corner where $\tilde{g}q' > 10^{-2}$ is needed to accommodate the Belle II data and thus the leading order expansion used for the Z' mixing is no longer valid. In this regime, $Z - Z'$ mixing is also expected to dominate $C_{\rm bs}^V$ in Eq. (21) and therefore the $B^+ \to K^+ Z'$ process. The scenario where Z' is produced via the $Z - Z'$ mixing and decays dominantly via $Z' \to \psi\bar{\psi}$ was considered previously in Ref. [22].[7]

B. Other phenomenology

Here, we review the other constraints shown in Fig. 8. The strongest bounds come from direct ATLAS and CMS searches for top partners [64], the CMS measurement of the top quark Yukawa coupling [65], and $e^+e^- \to \gamma Z'$ followed by $Z' \to$ inv at *BABAR* [66]. We give a summary of these and other constraints in the next few subsections.

1. Dark photon searches

Direct searches for dark photons with $M_{Z'} = 2.1$ GeV have been performed at *BABAR* [66,67], BESIII [68] and LHCb [69,70]. The most stringent bounds on the kinetic mixing ϵ_A are derived from a search for $e^+e^- \to \gamma Z'$, followed by $Z' \to e^+e^-/\mu^+\mu^-$ [67] or $Z' \to$ inv [66] at

[7]To evade the constraints on ϵ_A from dark photon searches at *BABAR*, discussed in the next section, the $Z - Z'$ mixing in this case must be induced principally by the mass mixing. The simplest model realization is an $SU(2)_L$ doublet scalar Φ' charged under $U(1)'$, with $\mathcal{L} \supset |D_\mu \Phi'|^2$ generating tree-level mass mixing between Z and Z' [22].

BABAR. The former process constrains the minimal $U(1)'$ scenario in Sec. II for large $\tilde{g}q'$. However, if $Z' \to \psi\bar{\psi}$ dominates the Z' decay width to accommodate the Belle II data, only the latter process is relevant in the parameter space of Fig. 8. We recast the bound as $\epsilon_A^2 \mathcal{B}(Z' \to \text{inv}) < 7.8 \times 10^{-4}$ (90% CL), with the exclusion shown as a purple shaded region in Fig. 8. Taking $\epsilon_A = -\epsilon_Z/t_w = e\tilde{g}q' L_T/6\pi^2$ and $\mathcal{B}(Z' \to \text{inv}) \approx 1$, we find that

$$\tilde{g}q' \gtrsim 2.7 \times 10^{-3} \left[\frac{55}{L_T}\right], \tag{41}$$

is approximately excluded by the *BABAR* data.

2. Collider searches

If light enough, the top partner T can be pair produced at the LHC, with the production cross section dominated by the QCD-induced $gg \to T\bar{T}$ partonic process. The final state, and therefore the signature probed by ATLAS or CMS experiments, depends on how T decays.

In Fig. 9, we illustrate the branching fractions of T as a function of y_T^t, for $m_T = 1.5$ TeV and $M_{Z'} = 2.1$ GeV. For $y_T^t \lesssim 0.2$, the branching fractions tend towards those of a typical $SU(2)_L$ singlet top partner. For $m_t \ll m_T$, the decay rates are $\Gamma(T \to \text{SM}) \approx m_T^2 s_L^2 C/32\pi v^2$ where $C \in \{2|V_{tb}|^2, 1, 1\}$ for $\text{SM} \in \{bW^+, tZ, th\}$, predicting $\mathcal{B}(T \to \text{SM}) \approx \{1/2, 1/4, 1/4\}$. Instead, for $y_T^t \gtrsim 0.2$, the Z' coupling dominates, with $\Gamma(T \to tZ') \approx m_T^2 s_R^2/32\pi\tilde{v}^2$ and $\mathcal{B}(T \to tZ') \approx 1$. For simplicity, we assume that the scalar ϕ is heavier than T, forbidding $T \to t\phi$ decays. For $M_\phi \ll m_T$, $T \to tZ'/t\phi$ would have equal decay rates.

In the $SU(2)_L$ singletlike limit, currently the most sensitive signature at the LHC is $pp \to T\bar{T} \to b\bar{b}W_l^\pm W_h^\mp$. Here, one final-state $W^\pm$ is required to decay leptonically, $W_l^\pm \to \ell^\pm\nu$ with $\ell = e, \mu$, suppressing SM processes with purely hadronic final states. The other $W_h^\pm$ decays hadronically, leading to the total final state containing one lepton, missing transverse energy (E_T^{miss}) and jets. With

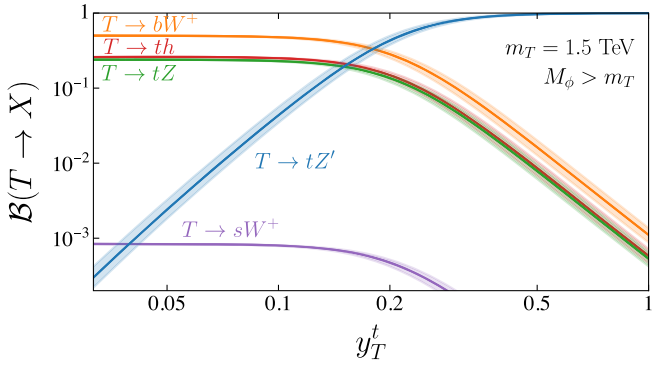

FIG. 9. Branching fractions of T satisfying the Belle II data in the minimal aligned $U(1)'$ plus ψ scenario, as a function of y_T^t for $m_T = 1.5$ TeV and assuming $M_\phi > m_T$.

$\mathcal{L} = 140$ fb^{-1} of Run 2 data, ATLAS performed a search [64] for such a final state, placing the lower bound $m_T > 1.36$ TeV (95% CL).

Instead, in the large Z' coupling limit, the most stringent signature is $pp \to T\bar{T} \to t\bar{t}Z'Z' \to t\bar{t} + E_T^{\text{miss}}$. We note that the Z' is expected to decay mostly invisibly in the $r_\psi = 12$ scenario, with $\mathcal{B}(Z' \to \psi\bar{\psi}) \approx 1$. The $t\bar{t} + E_{\text{miss}}$ final state is the focus of a number of ATLAS and CMS analyses, e.g., searches for pair-produced stops [71–73]. As there is no dedicated search for vectorlike top partners with this final state, we use the CheckMATE [74] package to recast these analyses. To this end, we create a FeynRules [75] model file to generate a UFO output for the model with a dark fermion. We then simulate $pp \to T\bar{T}$ events at next-to-leading order (NLO) in QCD using MadGraph5_aMC@NLO [76] and T decays using MadSpin [77], followed by showering and hadronization with Pythia 8 [78]. We rescale the obtained cross sections to the full next-to-next-to-leading order QCD results, as computed by TOP++ [79]. First, we simulate the case of both top partners decaying to a top quark and Z' (which most likely occurs on the rhs of Fig. 9) for T masses in the range $m_T \in [1, 2]$ TeV. We denote the obtained cross sections as $\sigma(pp \to (T \to tZ')(\bar{T} \to \bar{t}Z')) = \sigma_{tZ'}$. At each mass point we use CheckMATE to find the 95% CL upper limit on the cross section, constructing the ratio $\hat{\sigma}_{tZ'} = \sigma_{tZ'}^{\text{th}}/\sigma_{tZ'}^{95\%}$. We find that the scenario is excluded, i.e., $\hat{\sigma}_{tZ'} > 1$, for $m_T < 1.71$ TeV (95% CL) by the ATLAS search in Ref. [73]. Furthermore, we simulate the scenario of one top partner decaying to a top quark and Z' and the other to SM final states (bW^+, tZ, th), which is most probable in the transition region of Fig. 9. We likewise define the cross section $\sigma(pp \to (T \to tZ/th/bW^+)(\bar{T} \to \bar{t}Z')) + \sigma(pp \to (T \to tZ')(\bar{T} \to \bar{t}Z/\bar{t}h/\bar{b}W^-)) = \sigma_{\text{SM}/tZ'}$ and obtain the ratio $\hat{\sigma}_{\text{SM}/tZ'}$ for this scenario from CheckMATE. We find $\hat{\sigma}_{\text{SM}/tZ'} > 1$ for $m_T < 1.56$ TeV (95% CL) by the ATLAS search in Ref. [73]. Finally, for the scenario where both top partners decay to SM final states, we extract the ratio $\hat{\sigma}_{\text{SM}}$ from Fig. 5(b) of Ref. [64]. Now, we can exclude the parts of the parameter space at 95% CL where the ratio

$$R = \hat{\sigma}_{\text{SM}}\mathcal{B}_{\text{SM}}^2 + \hat{\sigma}_{\text{SM}/tZ'}\mathcal{B}_{\text{SM}}\mathcal{B}_{tZ'} + \hat{\sigma}_{tZ'}\mathcal{B}_{tZ'}^2, \tag{42}$$

satisfies $R > 1$, where $\mathcal{B}_X = \mathcal{B}(T \to X)$. The resulting exclusion is depicted as a dark blue region in Fig. 8. For $\tilde{g}q'$ values closer to the consistency constraint, $m_T > 1.36$ TeV, and for larger $\tilde{g}q'$ values, $m_T > 1.71$ TeV; this is expected from the scaling of y_T^t in the parameter space to explain the Belle II excess.

3. Higgs measurements

Another important constraint on the model arises from measurements of the top Yukawa coupling y_t. In our setup, y_t is determined from the input parameters $\{m_T, \tilde{g}q', y_T^t\}$ as $vy_t/\sqrt{2} = m_t c_L c_R + m_T s_L s_R$. Thus, the impact of $t - T$

mixing is a positive shift to the SM value $y_t^{\rm SM}$, such that the quantity $\kappa_t = y_t/y_t^{\rm SM}$ must lie in range $\kappa_t \in [1, \sqrt{m_T/m_t}]$. The strongest direct constraints on κ_t are from CMS [65], which searched for $pp \to t\bar{t}h$ followed by $h \to \tau^+\tau^-/W^+W^-/ZZ$, targeting final states with multiple electrons, muons, or hadronically decaying τ leptons. If the τ lepton Yukawa coupling is the same as the SM value, CMS finds $\kappa_t \in [0.7, 1.1]$ at 95% CL. The upper limit $\kappa_t < 1.1$ excludes a significant portion of the $(m_T, \tilde{g}q')$ parameter space, shown as a light green region in Fig. 8. Combining Eq. (39) with the expression for y_t in terms of the input parameters, we can derive that

$$\tilde{g}q' \lesssim 7.4 \times 10^{-5} \left[\frac{8.6}{X_t}\right], \tag{43}$$

is approximately excluded by the CMS κ_t measurement.

Finally, we comment on constraints on the model from Higgs decays. The potentially relevant interactions of the Higgs boson in the model are

$$\mathcal{L} \supset -s_\phi M_{Z'}^2 \frac{h}{\tilde{v}} Z'_\mu Z'^\mu + \frac{e}{16\pi^2} c_{h\gamma Z'} \frac{h}{v} F_{\mu\nu} Z'^{\mu\nu}. \tag{44}$$

The first is induced by $h - \phi$ mixing and can contribute to the decay $h \to Z'Z'$, with $\Gamma(h \to Z'Z') = m_h^3 s_\phi^2/32\pi\tilde{v}^2$, and to invisible Higgs decays ($h \to$ inv) if Z' decays are invisible. However, the scalar mixing depends on the value of M_ϕ, which we do not fix in Fig. 8, but require to lie in the range in Eq. (17) compatible with perturbative unitarity. For example, for $m_T = 10$ TeV and $y_T' = 1$, the value of $\tilde{g}q'$ implied by Belle II is just below the upper bound from *BABAR*. The allowed ϕ mass range here is $M_\phi \in [1.1, 4.2]$ TeV. We find that the upper bound $\mathcal{B}(h \to {\rm inv}) < 0.107$ (95% CL) [80] excludes this scenario only for $M_\phi < 1.9$ TeV. In the parameter space not excluded by the other constraints, we find that there are always values of M_ϕ not excluded by the constraint from $h \to$ inv. The second term in Eq. (44) is generated in the model via the kinetic and mass mixing and one-loop diagrams containing t/T, and induces $h \to \gamma Z'$ followed by $Z' \to$ inv. However, we verify that the bound $\mathcal{B}(h \to \gamma + {\rm inv}) < 0.013$ [81] is not competitive in the parameter space of Fig. 8.

4. Electroweak precision observables

As shown in Fig. 10, the heavy top partner contributes to the self-energies of the SM gauge fields and therefore to the parameters S, T, and U entering the predictions for electroweak precision observables (EWPOs), given by

$$\begin{aligned} S &= -\frac{1}{2\pi} s_L^2 \left[\frac{1}{3}\ln r + c_L^2 f(r)\right], \\ T &= -\frac{3}{8\pi s_w^2} \frac{m_t^2}{M_W^2} s_L^2 [1 - r + c_L^2 g(r)], \\ U &= \frac{1}{2\pi} s_L^2 [\ln r + c_L^2 f(r)], \end{aligned} \tag{45}$$

where the loop functions and their arguments have been defined previously in Sec. II A 2. In the relevant parameter space, we find that $T \gg S, U$. We may then use the best-fit value of the ρ parameter, $\rho \approx 1 + \alpha T = 1.00031 \pm 0.00019$ [82], which excludes the orange shaded region in Fig. 8. We note that the kinetic and mass mixing of Z' also contribute indirectly to the EWPOs, as they induce a small shift to the SM Z interactions and the input parameters M_Z and G_F [83–85]. However, this effect is expected to constrain only the parameter space with $\tilde{g}q' > 10^{-2}$, which is not considered in this work to maintain the validity of the leading-order expansion used for the Z' mixing. This region of parameter space is additionally excluded by the *BABAR* dark photon search.

Through the $Z - Z'$ mixing, the invisible Z decay width can be increased from the contribution of $Z \to \psi\bar{\psi}$. The decay rate is given by Eq. (37) with the replacements $\tilde{g}q'_\psi \to \tilde{g}q'_\psi \Delta_Z$ and $M_{Z'} \to M_Z$. The parameter space can then be constrained by the upper limit from large electron positron [86], $\Delta\Gamma_{\rm inv} < 2$ MeV (95% CL). However, the upper bound, which can be estimated as

$$\tilde{g}q' \lesssim 0.12 \left[\frac{12}{r_\psi}\right]^{1/2} \left[\frac{L_T}{55}\right]^{-1/2}, \tag{46}$$

is only stronger than the *BABAR* bound for very large values of the $U(1)'$ charge ratio, $r_\psi \gtrsim 10^4$, and therefore does not appear in Fig. 8. Other related probes which we have verified are less sensitive than the *BABAR* bound are the anomalous magnetic moment of the muon as well as atomic parity violation in cesium [87]. For example, the prediction for the Z' contribution to $a_\ell = (g-2)_\ell/2$ is $\Delta a_\ell = m_\ell^2[(v_{Z'}^\ell)^2 - 5(a_{Z'}^\ell)^2]/12\pi^2 M_{Z'}^2$. In the relevant region of the parameter space, we have $v_{Z'}^\ell \approx e\epsilon_A$ and $a_{Z'}^\ell \approx 0$ with $\epsilon_A = e\tilde{g}q' L_T/6\pi^2$, giving for $\ell = \mu$ and $M_{Z'} = 2.1$ GeV, as follows:

$$\Delta a_\mu = 1.5 \times 10^{-13} \left[\frac{\tilde{g}q'}{10^{-3}}\right]^2 \left[\frac{L_T}{55}\right]^2, \tag{47}$$

which is around 3 orders of magnitude below the current experimental sensitivity to a_μ and also well below the present uncertainties of SM theory predictions, which are both at the order of 10^{-10} [88,89]. The coupling $\tilde{g}q'$ is much

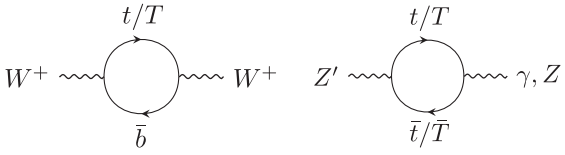

FIG. 10. One-loop contributions of the top partner to the self-energies of the SM gauge fields.

more tightly bound from above by the dark photon search at *BABAR*.

5. Other flavor probes

Here, we briefly review other potential flavor probes of the model and discuss why they are currently less sensitive than the bounds shown in Fig. 8. In principle, Z' can feature as a real or virtual state in other rare processes, since it couples to FCNC down-type quark currents in Eq. (19). However, for $M_{Z'} = 2.1$ GeV, Z' cannot be produced on shell from kaon decays. While $K \to \pi\psi\bar{\psi}$ via an off-shell Z' is kinematically possible for $2m_\psi < m_K - m_\pi$, we show in the next section that the viable region for ψ is outside this range. In particular, being stable and weakly coupled, ψ will necessarily decouple from the primordial plasma in the early Universe and form a thermal relic. In order not to overclose the Universe, its annihilation cross section should thus be sizeable enough. As we show in the next section, for $m_\psi < M_{Z'}/2$ as required by Belle II and LHCb, this is only possible close to the resonant condition $0.9 \lesssim m_\psi/\text{GeV} \lesssim 1$. At the boundary of the allowed region, ψ can actually constitute all of the observed DM. Thus, we do not consider much lower m_ψ values.

While the processes $B \to \pi Z'/\rho Z'$ are kinematically allowed, they are suppressed by V_{td}/V_{ts} with respect to $B \to K^{(*)}Z'$, and subject to similar upper bounds as $B \to K^* E_{\text{miss}}$ [90]. Next, we note that the heavy top partner T contributes at the one-loop level to rare SM processes via the charged- and neutral-current interactions in Eq. (6). For example, the $b \to s\gamma$ transitions as well as $B_{d,s}$ meson oscillations are modified in the model. However, since the one-loop contributions of T are always proportional to $s_L \ll s_R$, the current sensitivities are unable to constrain the relevant parameter space of the model in Fig. 8. In particular, EWPOs are always more constraining; see Ref. [91] for a more complete discussion. Finally, the model can also contribute to $B_{d,s} - \bar{B}_{d,s}$ oscillations via s- and t-channel Z' exchange. As the Z' is lighter than the meson masses, we can make use of the heavy-quark effective theory (HQET) formalism used in Ref. [92]. However, as the new contribution to the mass difference scales as $\Delta M_{d,s} \propto (C^V_{bs})^2$, we find for the value $C^V_{bs} = 1.4 \times 10^{-8}$ an effect which is 7 orders of magnitude smaller than the SM prediction.

C. Dark matter

The precise cosmic microwave background (CMB) measurements by the *Planck* Collaboration constitute an important constraint on the model, due to the presence of a stable ψ in the early Universe. Incidently, the measured relic abundance of DM $\Omega_{\text{DM}}h^2 = 0.120 \pm 0.001$ [93], can be readily accommodated in the model, with ψ constituting (part or) all of the DM ($\Omega_\psi \leq \Omega_{\text{DM}}$). Thus the measured DM relic abundance can be considered both as an opportunity and a constraint on the model.

The freeze-out of ψ in the early Universe is governed by the Boltzmann equation,

$$\frac{dY_\psi}{dx} = -\frac{s\langle\sigma v\rangle}{HxZ}(Y_\psi^2 - Y_{\psi,\text{eq}}^2), \tag{48}$$

where $x = m_\psi/T$, with T being the temperature of the thermal bath. Furthermore, $Y_\psi = n_\psi/s$ is the number density of ψ in units of the entropy density $s = 2\pi^2 h_{\text{eff}} T^3/45$ (with $Y_{\psi,\text{eq}}$ the equilibrium value), $H = \sqrt{8\pi\rho/3M_{\text{Pl}}^2}$ is the Hubble expansion rate with a radiation-dominated energy density $\rho = \pi^2 g_{\text{eff}} T^4/30$, $\langle\sigma v\rangle$ is the thermally averaged annihilation cross section of ψ into species still in thermal equilibrium, and $Z = (1 + \frac{1}{3} d\ln h_{\text{eff}}/d\ln T)^{-1}$ accounts for the rate of change of T. Above, $M_{\text{Pl}} = 1.22 \times 10^{19}$ GeV is the *Planck* mass and g_{eff} (h_{eff}) is the effective number of degrees of freedom for the energy (entropy) density.

We may solve Eq. (48) approximately as

$$\frac{1}{Y_\psi(x)} - \frac{1}{Y_f} = \sqrt{\frac{\pi}{45}} M_{\text{Pl}} m_\psi \int_{x_f}^{x} dx \frac{\sqrt{g_*}\langle\sigma v\rangle}{x^2}, \tag{49}$$

where $Y_f \equiv Y_{\psi,\text{eq}}(x_f)$, with x_f the freeze-out value of x, and $g_* \equiv h_{\text{eff}}^2/g_{\text{eff}}Z^2$. Then, the present day relic density of ψ can be determined as $\Omega_\psi h^2 = m_\psi s_0 Y_0/\rho_{\text{cr},0}$, with $Y_0 \equiv Y_\psi(x_0)$, or

$$\frac{1}{\Omega_\psi h^2} = \int_{x_f}^{x} dx \frac{\sqrt{g_*}}{x^2} \frac{\langle\sigma v\rangle}{2.0 \times 10^{-27}\ \text{cm}^3\,\text{s}^{-1}}, \tag{50}$$

where the critical energy density is $\rho_{\text{cr}} = 3M_{\text{Pl}}^2 H^2/8\pi$ and we account for nonidentical DM particles (ψ) and antiparticles ($\bar{\psi}$).

We are interested in the freeze-out of ψ for masses which can accommodate the Belle II excess, i.e., $m_\psi < M_{Z'}/2$. The dominant annihilation process in this mass range is $\psi\bar{\psi} \to \text{SM} + \text{SM}$ through s-channel Z' exchange, shown in Fig. 11 (left). The Z' couples at tree level to ψ and via the kinetic and mass mixing to light SM fields. As the annihilation can take place near the narrow Z' resonance, the thermally averaged cross section cannot be estimated using the typical nonrelativistic expansion in the relative DM velocity v. The thermally averaged Breit-Wigner cross section is s-wave dominated and given at leading order in $\epsilon_\psi \equiv (M_{Z'}^2 - 4m_\psi^2)/4m_\psi^2$ by [94]

$$\langle\sigma v\rangle = \frac{12\pi^{3/2}\gamma_{Z'}\mathcal{B}_{Z'}}{m_\psi^2} x^{3/2} e^{-x\epsilon_\psi}, \tag{51}$$

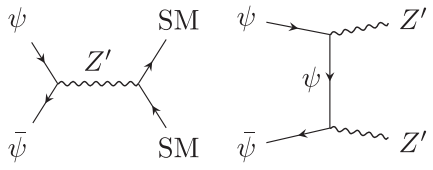

FIG. 11. Scattering processes contributing to the freeze-out of the DM candidate ψ.

defining $\gamma_{Z'} \equiv M_{Z'}\Gamma_{Z'}/4m_\psi^2$ and $\mathcal{B}_{Z'} \equiv \mathcal{B}_{\psi\bar{\psi}}\mathcal{B}_{\rm SM}$, where $\mathcal{B}_{\psi\bar{\psi}} = \Gamma_{\psi\bar{\psi}}/\Gamma_{Z'}$. With the vectorlike fermion ψ as the only light dark sector particle, $\mathcal{B}_{\rm SM} = 1 - \mathcal{B}_{\psi\bar{\psi}}$. Inserting Eq. (51) into Eq. (50) yields the approximate analytical result

$$\Omega_\psi h^2 = \frac{3.4 \times 10^{-12}\ \text{GeV}}{\Gamma_{Z'}} \frac{\sqrt{\hat{\epsilon}_\psi}}{\mathcal{B}_{Z'}}, \tag{52}$$

with $\hat{\epsilon}_\psi \equiv \epsilon_\psi/\bar{g}_*(1+\epsilon_\psi)^4 \text{erfc}^2(\sqrt{x_f\epsilon_\psi})$, where erfc is the complementary error function, g_* is fixed to its value at chemical decoupling, $\bar{g}_* = g_*(x_f)$, and we always assume that $M_{Z'} = 2.1$ GeV. In the limit where $\mathcal{B}_{\psi\bar{\psi}} \approx 1$ and the kinetic mixing ϵ_A dominates the Z' coupling to SM states, which generally holds when the Belle II excess is satisfied, Eq. (52) gives

$$\frac{\Omega_\psi}{\Omega_{\rm DM}} = \left[\frac{1.5 \times 10^{-4}}{\tilde{g}q'}\right]^2 \left[\frac{55}{L_T}\right]^2 \left[\frac{\hat{\epsilon}_\psi}{2.3}\right]^{1/2}, \tag{53}$$

using $x_f = 20$. Note that the result is independent of the $U(1)'$ charge ratio r_ψ. Using Eq. (39), the Belle II excess and the correct DM abundance can both be recovered for a specific value of m_T when the top partner Yukawa is

$$y_T^t = 0.29 \left[\frac{m_T}{10\ \text{TeV}}\right] \left[\frac{55}{L_T}\right]^{1/2} \left[\frac{8.6}{X_t}\right]^{1/2} \left[\frac{\hat{\epsilon}_\psi}{2.3}\right]^{1/8}. \tag{54}$$

To verify these estimates, we use the micrOMEGAs [95] package to compute Ω_ψ by numerically solving Eq. (48). We use FeynRules [75] to write CalcHEP [96] files for the same model file used in the collider analysis in Sec. III B, which are then implemented in micrOMEGAs.

In the top panel of Fig. 12, we show where in the $(m_T, \tilde{g}q')$ plane the correct DM relic abundance is obtained for four benchmark ϵ_ψ values, with $\epsilon_\psi = \{0.35, 0.20, 0.10, 0.02\}$ corresponding to $m_\psi \approx \{0.90, 0.96, 1.00, 1.04\}$ GeV. The bands indicate $\Omega_\psi = \Omega_{\rm DM} \pm 20\%$. Firstly, we find that Ω_ψ is well approximated by the scaling in Eq. (53) in this regime. Comparing the DM predictions to the region still allowed by the current constraints in Fig. 8, which are combined as a gray shaded region in Fig. 12 and are approximately independent of ϵ_ψ, lower and upper limits on ϵ_ψ are implied. A lower bound on ϵ_ψ is determined by the CMS bound on the top Yukawa coupling. Combining Eqs. (43) and (53), we find

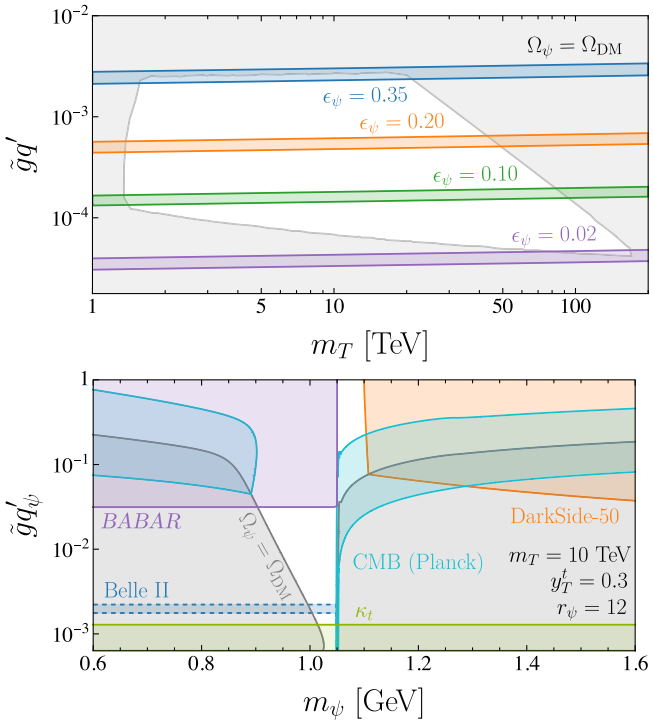

FIG. 12. Top: $(m_T, \tilde{g}q')$ parameter space where the correct DM relic abundance ($\Omega_\psi = \Omega_{\rm DM} \pm 20\%$) is obtained for different values of ϵ_ψ (color shaded bands). The unshaded region is the parameter space not excluded in Fig. 8, which can accommodate the Belle II excess. Bottom: bounds on the light ψ DM scenario in the $(m_\psi, \tilde{g}q'_\psi)$ plane. The correct DM relic abundance is found along the gray line, with DM overabundance obtained below. For $m_\psi < M_{Z'}/2$, there is a window where Belle II and *Planck* can be satisfied and the direct and indirect DM bounds are evaded. We show the constraints from *BABAR* (purple), the top Yukawa coupling (light green), *Planck* (light blue), and DarkSide-50 (orange).

$$\hat{\epsilon}_\psi \gtrsim 0.13 \left[\frac{L_T}{55}\right]^4 \left[\frac{8.6}{X_t}\right]^4, \tag{55}$$

which gives $\epsilon_\psi \gtrsim \{0.05, 0.02\}$ for $m_T = \{10, 150\}$ TeV, using the definition of $\hat{\epsilon}_\psi$ below Eq. (52). Upper bounds on ϵ_ψ are determined either by the *BABAR* bound from $e^+e^- \to \gamma Z'$ or the perturbative unitarity bound on the scalar sector. From the former, combining Eq. (41) with Eq. (53) yields $\epsilon_\psi \lesssim 0.35$, independent of m_T. The latter instead implies, using Eq. (40),

$$\hat{\epsilon}_\psi \lesssim 2.7 \times 10^7 \left[\frac{10\ \text{TeV}}{m_T}\right]^8 \left[\frac{X_t}{8.6}\right]^4, \tag{56}$$

giving $\epsilon_\psi \lesssim \{0.47, 0.04\}$ for $m_T = \{10, 150\}$ TeV. Thus, we find that for viable DM, $0.02 \lesssim \epsilon_\psi \lesssim 0.35$ is required.

Before moving on, we note that in the regime $\epsilon_\psi \ll 1$, i.e., very close to the Z' resonance, the abundance of ψ

evolves long after chemical decoupling at x_f in a belated freeze-out process [97]. Kinetic equilibrium between ψ and the SM bath cannot be maintained during this freeze-out, because nonresonant DM-SM scattering processes are suppressed. Thus, solving the Boltzmann equation in Eq. (48) no longer provides reliable results for $\Omega_\psi h^2$ [98]. The impact of kinetic decoupling on the DM abundance can be estimated, following the approach in Ref. [97], by multiplying Eq. (52) by the factor $k_{\rm dec} = 2\sqrt{\pi x_d \epsilon_\psi}$, where $x_d = m_\psi/T_d$, with T_d the temperature of kinetic decoupling. For a Z' satisfying $\gamma_{Z'} \lesssim 10^{-7}$, which is anticipated in the model for $\epsilon_\psi \ll 1$, $x_d \approx x_f$. However, we still find that $k_{\rm dec} > 1$ for the ϵ_ψ values in the range $0.02 \lesssim \epsilon_\psi \lesssim 0.35$, so the DM abundance is not suppressed by the kinetic decoupling.

To illustrate further the viable DM parameter space, we show in the bottom panel of Fig. 12 the relevant constraints in the $(m_\psi, \tilde{g}q'_\psi)$ plane for the benchmark values $m_T = 10$ TeV, $y_T^t = 0.3$ and $r_\psi = 12$. Unlike Figs. 8 and 12 (top panel), we do not require the Belle II excess to be accommodated at each point in the parameter space. For $m_\psi < M_{Z'}/2$, the favored region for Belle II is shown as a blue band. We also extend the mass range to $m_\psi > M_{Z'}/2$, where additional invisible Z' decays would need to be present to explain the Belle II result and be compatible with LHCb. We restrict to $m_\psi < M_{Z'}$ so that the s-channel process $\psi\bar{\psi} \to {\rm SM} + {\rm SM}$ still dominates the DM freeze-out. Firstly, the correct DM relic abundance is obtained along the gray solid line, while the gray shaded region below indicates the overproduction of DM. We show the bounds from *BABAR* and κ_t discussed in Secs. III B 1 and III B 2 which constrain $\tilde{g}q'$, in addition to the limits from (in)direct detection discussed below.

Relevant direct detection bounds in this mass range come from DarkSide-50, constraining DM (ψ) scattering on Ar [99]. For the parameter space shown in Fig. 12, the kinetic mixing ϵ_A dominates the interactions of Z' with the SM states. Thus, spin-independent (SI) scattering of ψ and protons via the exchange of Z' dominates the DM-Ar scattering cross section. Using micrOMEGAs, we compute at each point in the parameter space the ratio of the expected SI cross section to the 90% CL excluded value, $\hat{\sigma}_{\rm SI} = \sigma_{\rm SI}^{\rm th}/\sigma_{\rm SI}^{90\%}$, excluding $\hat{\sigma}_{\rm SI} > 1$ at 90% CL. If ψ makes up a faction of the observed DM abundance, we exclude $\hat{\sigma}_{\rm SI}(\Omega_\psi/\Omega_{\rm DM}) > 1$. The orange shaded region in Fig. 12 shows the resulting limit, excluding viable DM scenarios with $m_\psi > 1.1$ GeV in the mass range shown. Importantly, the most relevant region $m_\psi < M_{Z'}/2$ remains unconstrained.[8]

[8]There are also direct detection bounds from DM (ψ) scattering on electrons via Z' exchange, with XENON1T [100] and PandaX-4T [101] being the most stringent experiments. Similar to the nuclear scattering, the bounds are not relevant in the resonant regime in Fig. 12.

At recombination, the annihilation of ψ into SM states provides an indirect detection bound on the model. CMB anisotropies measured by *Planck* constrain the parameter $p_{\rm ann} < 3.2 \times 10^{-28}\ {\rm cm^3\,s^{-1}\,GeV^{-1}}$ (95% CL) [93], which is sensitive to energy injection from $e^\pm$ and γ produced by DM annihilation final states. We can estimate

$$p_{\rm ann} = \sum_i \frac{f_i^{\rm eff}\langle\sigma v\rangle_i}{m_\psi}\left(\frac{\Omega_\psi}{\Omega_{\rm DM}}\right)^2, \tag{57}$$

where, for the annihilation channel i, $f_i^{\rm eff}$ is the fraction of energy transferred to the plasma [102,103], $\langle\sigma v\rangle_i$ is the thermally averaged cross section, and we rescale by the fractional contribution of ψ to the total DM relic density. The scattering cross section is well approximated by the zero velocity limit expression,

$$\langle\sigma v\rangle_i = \frac{6\pi\gamma_{Z'}^2\mathcal{B}_{\psi\bar{\psi}}\mathcal{B}_i}{m_\psi^2\sqrt{\epsilon_\psi}(\gamma_{Z'}^2+\epsilon_\psi^2)}. \tag{58}$$

Using micrOMEGAs, the $f_i^{\rm eff}$ and $\langle\sigma v\rangle_i$ are computed and the parameter space excluded by the *Planck* upper limit is shown as a light blue shaded region in Fig. 12. For ϵ_ψ sufficiently large, and thus below the resonance, the $\langle\sigma v\rangle_i$ are suppressed enough for the CMB bound to be evaded. Note that for masses in this range, the e^+ and γ spectra calculated in micrOMEGAs, which act as input to $f_i^{\rm eff}$, carry significant uncertainties. Hadronization of the quark final states is calculated using Pythia and extrapolated to lower masses, where hadronic resonances make the Pythia calculations less reliable. Nevertheless, we do not expect this to make up for the large suppression of $\langle\sigma v\rangle_i$ below the resonance at recombination. The late time annihilation of DM to SM particles is similarly suppressed, and therefore indirect detection bounds, e.g., from Super-Kamiokande [104] or x-ray data [105,106], are evaded.

To conclude, the resonant thermal annihilation of ψ in the early Universe for $0.9 \lesssim m_\psi/{\rm GeV} \lesssim 1.0$ GeV, where ψ simultaneously appear as missing energy at Belle II, offers a compelling DM scenario which is not yet experimentally excluded by direct or indirect detection. The model presented offers the minimal field content to fit both the Belle II data and generate the correct relic abundance with a light Z'. Of course, the presence of additional fields in an extended dark sector charged under $U(1)'$ would modify the DM phenomenology, as we discuss briefly in the next section.

IV. DISCUSSION AND CONCLUSIONS

In previous work [2,4], we demonstrated within a model-independent EFT framework that the Belle II excess in $B^+ \to K^+ E_{\rm miss}$ can be well described by the emission of a single light vector boson, with a mass of about

$M_{Z'} \simeq 2.1$ GeV, in $b \to s$ transitions. We have now extended this to a simple UV-complete construction, based on a Higgsed $U(1)'$ gauge symmetry with a light vector boson Z', a complex scalar Φ whose vacuum expectation value gives mass to Z', and a $U(1)'$ charged vectorlike top partner T realising a rank-1 pattern of flavor breaking, aligned to the third generation, that naturally enhances $b \to s$ processes.

In this minimal construction, loop-induced $b \to sZ'$ transitions generate the desired Belle II signal through a left-handed current operator, but the same loops unavoidably induce kinetic and mass mixing between Z' and the electroweak gauge bosons, leading to irreducible couplings of Z' to charged leptons that cannot even be fine-tuned away. The resulting branching ratios in the minimal model, displayed in Fig. 5, show that Z' decays dominantly into visible SM final states, with a sizeable $\mu^+\mu^-$ branching fraction in the parameter region favored by Belle II. The corresponding contributions to $B \to K^{(*)}\mu^+\mu^-$ are excluded by existing LHCb searches for prompt and displaced dimuon resonances (Fig. 6). We therefore conclude that the minimal aligned $U(1)'$ model cannot account for the Belle II anomaly; its failure is directly tied to the absence of sufficiently large invisible Z' decay channels as the Z' effectively always decays inside the detector.

Motivated by this, we extended the $U(1)'$ charged sector by adding a light SM singlet fermion ψ, which opens a dominant invisible decay mode $Z' \to \psi\bar{\psi}$ and sufficiently suppresses the visible branching ratios (provided the $\psi U(1)'$ charge is an order of magnitude larger than that of T and Φ), as seen in the modified decay patterns in Fig. 7. The same interaction controls the ψ annihilation rate in the early Universe, and a combination of flavor, collider, electroweak, and cosmological constraints selects a narrow ψ mass regime, just below half of the Z' mass, illustrated in Fig. 12, where ψ can constitute part or all of DM. Outside this resonant region, the model violates at least one of these constraints. Future improved measurements and searches, planned at existing and upcoming experimental facilities like Belle II [107] and future circular collider [108], will be able to further constrain the viable parameter space. The model thus represents a highly constrained and predictive scenario relating missing energy signatures in rare B decays to a comprehensive collider and DM phenomenology.

Extensions of the model field content could potentially relax some of the constraints found in the minimal model. For instance, the large $U(1)'$ charge ratio (r_ψ) between ψ and T, Φ could be avoided by considering multiple light dark fermions ψ_i with $r_{\psi_i} \sim 1$ instead of one ψ with $r_\psi \gg 1$. Secondly, the CMB and direct detection constraints could be further relaxed for dark fermions with axial-vector couplings to the Z'. Such a scenario would be obtained if different $U(1)'$ charges are assigned to the left- and right-handed components $\psi_L \equiv \psi$ and $\psi_R \equiv \psi'$. For example, with $q'_L \equiv q'_\psi \neq q'_R = q'_{\psi'}$, we have

$$\mathcal{L} \supset \bar{\psi} i \not{D} \psi + \overline{\psi'} i \not{D} \psi' - \frac{1}{2}\left[Y_\psi \overline{\psi'^c} \psi' \tilde{\Phi} + \text{H.c.} \right], \tag{59}$$

where $\psi^c = C\bar{\psi}^T$, with C the charge conjugation matrix, and we also introduce the scalar $\tilde{\Phi} = (\tilde{v}_\psi + \varphi + ia)/\sqrt{2}$ with the $U(1)'$ charge $-2q'_R$. In the broken $U(1)'$ phase, the Majorana mass $m_{\psi'} = \tilde{v}_\psi Y_\psi/\sqrt{2}$ is generated for ψ'. The state ψ may also be a Majorana fermion if the charges obey $q' = q'_L - q'_R$, thus permitting the Yukawa coupling

$$\mathcal{L} \supset -y_\psi \bar{\psi} \psi' \Phi + \text{H.c.}. \tag{60}$$

For $\tilde{v} y_\psi \ll \tilde{v}_\psi Y_\psi$, a seesawlike mechanism generates a Majorana mass for ψ of size $m_\psi \approx (\tilde{v} y_\psi)^2/(\sqrt{2}\tilde{v}_\psi Y_\psi)$. In this setup, both ψ and ψ' have purely axial-vector couplings to Z' and their annihilation would be p-wave (v^2-suppressed), reducing $\langle \sigma v \rangle$ at recombination by $\sim (v_{\rm CMB}/v_{\rm fo})^2 \sim 10^{-6}$, while maintaining efficient freeze-out. The annihilation then proceeds either through the Z' resonance for $m_{\psi^{(\prime)}} \lesssim M_{Z'}/2$ or alternatively for $m_{\psi^{(\prime)}} \gtrsim M_{Z'}$ through the process $\psi^{(\prime)}\psi^{(\prime)} \to Z'Z'$ shown in Fig. 11 (right). In such an extended scenario, the missing energy at Belle II can either be provided by the $\psi^{(\prime)}$ fields, $Z' \to \psi^{(\prime)}\psi^{(\prime)}$, or alternatively the physical CP-even and -odd components of Φ and $\tilde{\Phi}$ (mass eigenstates φ' and a'), $Z' \to \varphi' a'$, if they are sufficiently light. We leave such considerations for future work.

ACKNOWLEDGMENTS

The authors would like to thank Svjetlana Fajfer for her contributions in the initial stages of this work, and Zara Barbarić for her assistance in deriving the collider bounds on the model. We thank Alexander Belyaev for his assistance with micrOMEGAs in the early stages of the project. We also thank Genevieve Belanger and Cedric Delaunay for their insightful correspondence regarding Ref. [97] and micrOMEGAs, and Marco Ardu for his comments regarding p-wave annihilation. P. D. B. and J. F. K. acknowledge financial support from the Slovenian Research Agency (research core funding No. P1-0035 and No. N1-0321). M. N. acknowledges the financial support of the Spanish Government (Agencia Estatal de Investigación MCIN/AEI/10.13039/501100011033) and the European Union NextGenerationEU/PRTR through the "Juan de la Cierva" program (Grant No. JDC2022-048787-I) and through Grants No. PID2020–114473GB-I00 and No. PID2023-146220NB-I00.

DATA AVAILABILITY

The data that support the findings of this article are not publicly available upon publication because it is not technically feasible and/or the cost of preparing, depositing, and hosting the data would be prohibitive within the terms

of this research project. The data are available from the authors upon reasonable request.

APPENDIX: FULL FORMULAS

Here, we give the full matching relations for the WET coefficients in Eq. (18). Firstly, the coupling of Z' to the left-handed vector down-type quark current is

$$C_{ij}^V(M_W) = \frac{1}{2}\mathcal{C}_{ij} m_t^2 c_L^2 \left[\tilde{g} q' s_R^2 C_{Z'}^V - \frac{g}{c_w}\Delta_{Z'} C_Z^V\right], \quad \text{(A1)}$$

at $\mu = M_W$, with

$$\begin{aligned} C_{Z'}^V &= X(x_t) + X(x_T) + X'(x_t, x_T) + \frac{2s_L^2}{s_R^2} g(r), \\ C_Z^V &= Y(x_t) + t_L^2 r Y(x_T) - s_L^2 g(r), \end{aligned} \quad \text{(A2)}$$

where $x_{t,T} = m_{t,T}^2/M_W^2$, $r = m_T^2/m_t^2$, the loop function $g(x)$ is defined below Eq. (10) and we define the additional loop functions as follows:

$$\begin{aligned} X(x) &= -\frac{x-4}{x-1} - \frac{x^2-2x+4}{(x-1)^2}\ln x, \\ X'(x,y) &= \frac{x-4}{x-1}\frac{2x}{x-y}\ln x + (x \leftrightarrow y), \\ Y(x) &= \frac{x-6}{x-1} + \frac{3x+2}{(x-1)^2}\ln x. \end{aligned} \quad \text{(A3)}$$

In the limit where $m_t \ll m_T$ and $\tilde{g} q'$ is sufficiently above the consistency bound in Eq. (5), $s_L^2 \approx s_R^2/r \ll 1$ yields the estimates $C_{Z'}^V \approx X(x_t) + \ln x_T + 1 \approx \ln x_T - 1$, where we used $X(x_t) = -2.05$, and $C_Z^V \approx Y(x_t) = 1.47$. For $m_t \ll m_T$ and $\tilde{g} q'$ close to the consistency bound, we instead have $s_L \approx 1/\sqrt{r}$ and $s_R \approx 1$, giving $C_{Z'}^V \approx 2\sqrt{r}$ and $C_Z^V \approx Y(x_t) + 1 = 2.47$. In these two limits, C_{ij}^V is given by Eqs. (21) and (22), respectively, which are used to derive approximate results in the text. However, we use the full expression in Eq. (A1) for the numerical studies of this analysis.

The coupling of Z' to the dipolelike down-type quark current is given at $\mu = M_W$ by

$$C_{ij}^T(M_W) = \mathcal{C}_{ij} m_i x_t c_L^2 \left[\tilde{g} q' s_R^2 C_{Z'}^T - e\epsilon_A C_\gamma^T - \frac{g}{c_w}\Delta_{Z'} C_Z^T\right], \quad \text{(A4)}$$

with

$$\begin{aligned} C_{Z'}^T &= A(x_t) + A(x_T) + A'(x_t, x_T) + \frac{s_L^2}{s_R^2 x_t} A''(x_t, x_T), \\ C_\gamma^T &= B(x_t) + t_L^2 r B(x_T), \\ C_Z^T &= C(x_t) + t_L^2 r C(x_T) + \frac{s_L^2}{x_t} C''(x_t, x_T) - s_w^2 C_\gamma^T, \end{aligned} \quad \text{(A5)}$$

where the relevant loop functions are

$$\begin{aligned} A(x) &= \frac{x^2-5x-2}{24(x-1)^3} + \frac{x}{4(x-1)^4}\ln x, \\ B(x) &= \frac{8x^2+5x-7}{24(x-1)^3} - \frac{3x^2-2x}{4(x-1)^4}\ln x, \\ C(x) &= \frac{5x^2+x}{16(x-1)^3} - \frac{5x^2-3x+1}{8(x-1)^4}\ln x, \end{aligned} \quad \text{(A6)}$$

and

$$\begin{aligned} A'(x,y) &= \frac{xy-1}{12(x-1)^2(y-1)^2} \\ &\quad - \frac{x^3-3x^2}{12(x-1)^3(x-y)}\ln x + (x \leftrightarrow y), \\ A''(x,y) &= -\frac{5x^2+5x-4}{12(x-1)^3} + \frac{2x^2-x}{2(x-1)^4}\ln x \\ &\quad + \frac{4xy-3x-3y+2}{6(x-1)^2(y-1)^2} \\ &\quad + \frac{5x^3-3x^2}{6(x-1)^3(x-y)}\ln x + (x \leftrightarrow y), \\ C''(x,y) &= \frac{7x^2+10x-5}{48(x-1)^3} - \frac{3x^2-x}{8(x-1)^4}\ln x \\ &\quad - \frac{13x-5}{48(x-1)^2(y-1)} \\ &\quad - \frac{7x^3-3x^2}{24(x-1)^3(x-y)}\ln x + (x \leftrightarrow y). \end{aligned} \quad \text{(A7)}$$

[1] I. Adachi *et al.* (Belle-II Collaboration), Phys. Rev. D **109**, 112006 (2024).
[2] P. D. Bolton, S. Fajfer, J. F. Kamenik, and M. Novoa-Brunet, Phys. Rev. D **110**, 055001 (2024).
[3] G. de Marino and L. E. Gaertner, in *2025 Belle II Physics Week* (KEK, Tsukuba, 2025) conference contribution.
[4] P. D. Bolton, S. Fajfer, J. F. Kamenik, and M. Novoa-Brunet, Phys. Rev. D **112**, 035010 (2025).
[5] J. F. Kamenik and C. Smith, Phys. Lett. B **680**, 471 (2009).
[6] K. Fridell, M. Ghosh, T. Okui, and K. Tobioka, Phys. Rev. D **109**, 115006 (2024).
[7] G. Guedes and P. Olgoso, arXiv:2412.14253.
[8] A. J. Buras, J. Harz, and M. A. Mojahed, J. High Energy Phys. 10 (2024) 087.
[9] S. Rosauro-Alcaraz and L. P. S. Leal, Eur. Phys. J. C **84**, 795 (2024).
[10] D. Marzocca, M. Nardecchia, A. Stanzione, and C. Toni, Eur. Phys. J. C **84**, 1217 (2024).
[11] B.-F. Hou, X.-Q. Li, M. Shen, Y.-D. Yang, and X.-B. Yuan, J. High Energy Phys. 06 (2024) 172.
[12] J. F. Kamenik, Y. Soreq, and J. Zupan, Phys. Rev. D **97**, 035002 (2018).
[13] V. Gherardi, D. Marzocca, M. Nardecchia, and A. Romanino, J. High Energy Phys. 10 (2019) 112.
[14] G. D'Ambrosio, G. F. Giudice, G. Isidori, and A. Strumia, Nucl. Phys. **B645**, 155 (2002).
[15] R. Barbieri, G. Isidori, J. Jones-Perez, P. Lodone, and D. M. Straub, Eur. Phys. J. C **71**, 1725 (2011).
[16] R. Barbieri, D. Buttazzo, F. Sala, and D. M. Straub, J. High Energy Phys. 07 (2012) 181.
[17] D. McKeen, J. N. Ng, and D. Tuckler, Phys. Rev. D **109**, 075006 (2024).
[18] W. Altmannshofer, A. Crivellin, H. Haigh, G. Inguglia, and J. Martin Camalich, Phys. Rev. D **109**, 075008 (2024).
[19] A. Berezhnoy and D. Melikhov, Europhys. Lett. **145**, 14001 (2024).
[20] W. Altmannshofer and S. Roy, Phys. Rev. D **111**, 075029 (2025).
[21] S.-Y. Ho, J. Kim, and P. Ko, Phys. Rev. D **111**, 055029 (2025).
[22] L. Calibbi, T. Li, L. Mukherjee, and M. A. Schmidt, Phys. Rev. D **112**, 075020 (2025).
[23] A. Berezhnoy, W. Lucha, and D. Melikhov, Phys. Rev. D **111**, 075035 (2025).
[24] L. Di Luzio, M. Nardecchia, and C. Toni, Phys. Rev. D **112**, 055031 (2025).
[25] J. Kim and P. Ko, arXiv:2511.20430.
[26] T. M. Aliev, A. Elpe, L. Selbuz, and I. Turan, Phys. Rev. D **112**, 015025 (2025).
[27] A. Datta, D. Marfatia, and L. Mukherjee, Phys. Rev. D **109**, L031701 (2024).
[28] C.-H. Chen and C.-W. Chiang, Phys. Rev. D **109**, 075004 (2024).
[29] X.-G. He, X.-D. Ma, and G. Valencia, Phys. Rev. D **109**, 075019 (2024).
[30] Z. S. Wang, H. K. Dreiner, and J. Y. Günther, Eur. Phys. J. C **85**, 66 (2025).
[31] T. Felkl, A. Giri, R. Mohanta, and M. A. Schmidt, Eur. Phys. J. C **83**, 1135 (2023).
[32] P. Athron, R. Martinez, and C. Sierra, J. High Energy Phys. 02 (2024) 121.
[33] B. Bhattacharya, A. Datta, G. Faisel, S. Khalil, and S. Roy, arXiv:2412.16115.
[34] A. J. Buras and P. Stangl, Eur. Phys. J. C **85**, 519 (2025).
[35] D. Bečirević, S. Fajfer, N. Košnik, and L. Pavičić, Phys. Lett. B **861**, 139285 (2025).
[36] C. Hati, J. Leite, N. Nath, and J. W. F. Valle, Phys. Rev. D **111**, 015038 (2025).
[37] C. S. Kim, D. Sahoo, and K. N. Vishnudath, Eur. Phys. J. C **84**, 882 (2024).
[38] X.-G. He, X.-D. Ma, M. A. Schmidt, G. Valencia, and R. R. Volkas, J. High Energy Phys. 07 (2024) 168.
[39] C.-H. Chen and C.-W. Chiang, Phys. Rev. D **110**, 075036 (2024).
[40] E. Gabrielli, L. Marzola, K. Müürsepp, and M. Raidal, Eur. Phys. J. C **84**, 460 (2024).
[41] F. Loparco, Particles **7**, 161 (2024).
[42] C.-H. Chen, C.-W. Chiang, and L. M. G. de la Vega, J. High Energy Phys. 09 (2025) 055.
[43] A. Crivellin, S. Iguro, and T. Kitahara, Phys. Rev. D **112**, 095016 (2025).
[44] R. Aaij *et al.* (LHCb Collaboration), Phys. Rev. Lett. **115**, 161802 (2015).
[45] R. Aaij *et al.* (LHCb Collaboration), Phys. Rev. D **95**, 071101 (2017).
[46] L. Allwicher, P. Arnan, D. Barducci, and M. Nardecchia, J. High Energy Phys. 10 (2021) 129.
[47] M. Bauer and P. Foldenauer, Phys. Rev. Lett. **129**, 171801 (2022).
[48] B. W. Lee, C. Quigg, and H. B. Thacker, Phys. Rev. D **16**, 1519 (1977).
[49] B. W. Lee, C. Quigg, and H. B. Thacker, Phys. Rev. Lett. **38**, 883 (1977).
[50] A. Bharucha, D. M. Straub, and R. Zwicky, J. High Energy Phys. 08 (2016) 098.
[51] N. Gubernari, M. Reboud, D. van Dyk, and J. Virto, J. High Energy Phys. 12 (2023) 153; 01 (2025) 125(E).
[52] Y. Ohnishi *et al.*, Prog. Theor. Exp. Phys. **2013**, 03A011 (2013).
[53] K. G. Chetyrkin, J. H. Kuhn, and A. Kwiatkowski, Phys. Rep. **277**, 189 (1996).
[54] P. A. Baikov, K. G. Chetyrkin, J. H. Kuhn, and J. Rittinger, Phys. Rev. Lett. **108**, 222003 (2012).
[55] A. Freitas, J. High Energy Phys. 04 (2014) 070.
[56] P. Ilten, Y. Soreq, M. Williams, and W. Xue, J. High Energy Phys. 06 (2018) 004.
[57] M. Bauer, P. Foldenauer, and J. Jaeckel, J. High Energy Phys. 07 (2018) 094.
[58] C. Baruch, P. Ilten, Y. Soreq, and M. Williams, J. High Energy Phys. 11 (2022) 124.
[59] A. L. Foguel, P. Reimitz, and R. Z. Funchal, J. High Energy Phys. 04 (2022) 119.
[60] J. P. Lees *et al.* (*BABAR* Collaboration), Phys. Rev. D **87**, 112005 (2013).
[61] M. Abumusabh *et al.* (Belle-II Collaboration), arXiv:2511.10980.
[62] R. Aaij *et al.* (LHCb Collaboration), J. High Energy Phys. 06 (2014) 133.

[63] S. Choudhury *et al.* (BELLE Collaboration), J. High Energy Phys. 03 (2021) 105.
[64] G. Aad *et al.* (ATLAS Collaboration), Phys. Lett. B **854**, 138743 (2024).
[65] A. M. Sirunyan *et al.* (CMS Collaboration), Eur. Phys. J. C **81**, 378 (2021).
[66] J. P. Lees *et al.* (*BABAR* Collaboration), Phys. Rev. Lett. **119**, 131804 (2017).
[67] J. P. Lees *et al.* (*BABAR* Collaboration), Phys. Rev. Lett. **113**, 201801 (2014).
[68] M. Ablikim *et al.* (BESIII Collaboration), Phys. Lett. B **774**, 252 (2017).
[69] R. Aaij *et al.* (LHCb Collaboration), Phys. Rev. Lett. **120**, 061801 (2018).
[70] R. Aaij *et al.* (LHCb Collaboration), Phys. Rev. Lett. **124**, 041801 (2020).
[71] G. Aad *et al.* (ATLAS Collaboration), J. High Energy Phys. 03 (2024) 139.
[72] G. Aad *et al.* (ATLAS Collaboration), Eur. Phys. J. C **83**, 561 (2023).
[73] G. Aad *et al.* (ATLAS Collaboration), Eur. Phys. J. C **80**, 737 (2020).
[74] M. Drees, H. Dreiner, D. Schmeier, J. Tattersall, and J. S. Kim, Comput. Phys. Commun. **187**, 227 (2015).
[75] A. Alloul, N. D. Christensen, C. Degrande, C. Duhr, and B. Fuks, Comput. Phys. Commun. **185**, 2250 (2014).
[76] J. Alwall, R. Frederix, S. Frixione, V. Hirschi, F. Maltoni, O. Mattelaer, H. S. Shao, T. Stelzer, P. Torrielli, and M. Zaro, J. High Energy Phys. 07 (2014) 079.
[77] P. Artoisenet, R. Frederix, O. Mattelaer, and R. Rietkerk, J. High Energy Phys. 03 (2013) 015.
[78] T. Sjostrand, S. Mrenna, and P. Z. Skands, Comput. Phys. Commun. **178**, 852 (2008).
[79] M. Czakon and A. Mitov, Comput. Phys. Commun. **185**, 2930 (2014).
[80] G. Aad *et al.* (ATLAS Collaboration), Phys. Lett. B **842**, 137963 (2023).
[81] G. Aad *et al.* (ATLAS Collaboration), J. High Energy Phys. 08 (2024) 153.
[82] S. Navas *et al.* (Particle Data Group), Phys. Rev. D **110**, 030001 (2024).
[83] K. S. Babu, C. F. Kolda, and J. March-Russell, Phys. Rev. D **57**, 6788 (1998).
[84] A. Hook, E. Izaguirre, and J. G. Wacker, Adv. High Energy Phys. **2011**, 859762 (2011).
[85] D. Curtin, R. Essig, S. Gori, and J. Shelton, J. High Energy Phys. 02 (2015) 157.
[86] S. Schael *et al.* (ALEPH, DELPHI, L3, OPAL, SLD Collaborations, LEP Electroweak Working Group, SLD Electroweak Group, SLD Heavy Flavour Group), Phys. Rep. **427**, 257 (2006).
[87] H. Davoudiasl, H.-S. Lee, and W. J. Marciano, Phys. Rev. D **85**, 115019 (2012).
[88] D. P. Aguillard *et al.* (Muon g-2 Collaboration), Phys. Rev. Lett. **135**, 101802 (2025).
[89] R. Aliberti *et al.*, Phys. Rep. **1143**, 1 (2025).
[90] J. Grygier *et al.* (Belle Collaboration), Phys. Rev. D **96**, 091101 (2017); **97**, 099902(A) (2018).
[91] S. Fajfer, A. Greljo, J. F. Kamenik, and I. Mustac, J. High Energy Phys. 07 (2013) 155.
[92] M. Bauer, M. Neubert, S. Renner, M. Schnubel, and A. Thamm, J. High Energy Phys. 09 (2022) 056.
[93] N. Aghanim *et al.* (Planck Collaboration), Astron. Astrophys. **641**, A6 (2020); **652**, C4(E) (2021).
[94] P. Gondolo and G. Gelmini, Nucl. Phys. **B360**, 145 (1991).
[95] G. Alguero, G. Belanger, F. Boudjema, S. Chakraborti, A. Goudelis, S. Kraml, A. Mjallal, and A. Pukhov, Comput. Phys. Commun. **299**, 109133 (2024).
[96] A. Belyaev, N. D. Christensen, and A. Pukhov, Comput. Phys. Commun. **184**, 1729 (2013).
[97] G. Bélanger, S. Chakraborti, C. Delaunay, and M. Jomain, Phys. Rev. D **112**, 095039 (2025).
[98] T. Binder, T. Bringmann, M. Gustafsson, and A. Hryczuk, Phys. Rev. D **96**, 115010 (2017); **101**, 099901(E) (2020).
[99] P. Agnes *et al.* (DarkSide Collaboration), Phys. Rev. Lett. **121**, 081307 (2018).
[100] E. Aprile *et al.* (XENON Collaboration), Phys. Rev. Lett. **123**, 251801 (2019).
[101] S. Li *et al.* (PandaX Collaboration), Phys. Rev. Lett. **130**, 261001 (2023).
[102] T. R. Slatyer, Phys. Rev. D **93**, 023527 (2016).
[103] R. K. Leane, T. R. Slatyer, J. F. Beacom, and K. C. Y. Ng, Phys. Rev. D **98**, 023016 (2018).
[104] K. Abe *et al.* (Super-Kamiokande Collaboration), Phys. Rev. D **102**, 072002 (2020).
[105] M. Cirelli, N. Fornengo, J. Koechler, E. Pinetti, and B. M. Roach, J. Cosmol. Astropart. Phys. 07 (2023) 026; 08 (2025) E02(E).
[106] S. Balaji, D. Cleaver, P. De la Torre Luque, and M. Michailidis, J. Cosmol. Astropart. Phys. 11 (2025) 053.
[107] W. Altmannshofer *et al.* (Belle-II Collaboration), Prog. Theor. Exp. Phys. **2019**, 123C01 (2019); **2020**, 029201(E) (2020).
[108] A. Abada *et al.* (FCC Collaboration), Eur. Phys. J. C **79**, 474 (2019).